

¹ **The paleogeography of Laurentia in its early years: new
2 constraints from the Paleoproterozoic East-Central
3 Minnesota batholith**

⁴ Nicholas L. Swanson-Hysell¹, Margaret S. Avery¹, Yiming Zhang¹, Eben B.
⁵ Hodgin¹, Robert J. Sherwood¹, Francisco E. Apen², Terrence J. Boerboom³,
⁶ C. Brenhin Keller^{1,4,5}, John M. Cottle²

⁷ ¹Department of Earth and Planetary Science, University of California, Berkeley, CA, USA

⁸ ²Department of Earth Science, University of California, Santa Barbara, CA, USA

⁹ ³Minnesota Geological Survey, St. Paul, MN, USA

¹⁰ ⁴Berkeley Geochronology Center, 2455 Ridge Road, Berkeley, CA, USA

¹¹ ⁵Department of Earth Sciences, Dartmouth College, Hanover, NH, USA

¹² **Key Points:**

- ¹³ • A new *ca.* 1780 Ma paleomagnetic pole reconstructs the Superior province of Lau-
rentia to moderately high latitudes
- ¹⁴ • This pole establishes the coherency of the Laurentia craton following Trans-Hudson
orogenesis and supports the NENA connection with Baltica
- ¹⁵ • Paleomagnetic and geologic data from Laurentia strongly support mobile-lid plate
tectonics from 2.2 Ga to the present day
- ¹⁶
- ¹⁷
- ¹⁸

19 **Abstract**

20 The *ca.* 1.83 Ga Trans-Hudson orogeny resulted from collision of an upper plate
 21 consisting of the Hearne, Rae, and Slave provinces with a lower plate consisting of the
 22 Superior province. While the geologic record of *ca.* 1.83 Ga peak metamorphism within
 23 the orogen suggests that these provinces should be considered as a single amalgamated
 24 craton from this time onward, a lack of paleomagnetic poles from the Superior province
 25 following Trans-Hudson orogenesis has made this coherency difficult to test. We develop
 26 a high-quality paleomagnetic pole for northeast-trending diabase dikes of the post-Penokean
 27 orogen East-Central Minnesota Batholith (pole longitude: 265.8° ; pole latitude: 20.4° ;
 28 A₉₅: 4.5° ; K: 45.6° N: 23) whose age we constrain to be 1779.1 ± 2.3 Ma (95% CI) with
 29 new U-Pb dates on the granites. Demagnetization and low-temperature magnetometry
 30 experiments establish the remanence of the dikes to be held by low-Ti titanomagnetite.
 31 Thermochronology data constrain these post-orogenic plutons to have cooled below mag-
 32 netite blocking temperatures upon initial emplacement and to have had a mild subse-
 33 quent thermal history within the stable craton with no evidence of any significant sub-
 34 sequent thermal overprinting. The similarity of this new Superior province pole with poles
 35 from the Slave and Rae provinces establishes the coherency of the Laurentia craton fol-
 36 lowing Trans-Hudson orogenesis. This consistency supports interpretations that older
 37 discrepant 2.22 to 1.87 Ga pole positions between the provinces are the result of differ-
 38 ential motion through mobile-lid plate tectonics. The East-Central Minnesota Batholith
 39 pole supports the NENA connection between the Laurentia and Fennoscandia cratons.
 40 The pole can be used to jointly reconstruct the paleogeographic positions of these cra-
 41 tons *ca.* 1780 Ma strengthening the position of these major constituents of the hypoth-
 42 esized late Paleoproterozoic supercontinent Nuna.

43 **1 Introduction**

44 In the Orosirian Period of the Paleoproterozoic Era, a series of collisional oroge-
 45 nies led to the amalgamation of Archean provinces to form the core of the Laurentia cra-
 46 ton (Fig. 1; Hoffman (1988); Whitmeyer and Karlstrom (2007)). The most significant
 47 of these orogenies was the *ca.* 1850 to 1800 Ma Trans-Hudson orogeny associated with
 48 the collision between the Superior province and the Churchill province which comprised
 49 a composite of the Slave, Hearne and Rae provinces (Fig. 1; Weller and St-Onge (2017)).
 50 The length of the orogen as well as the pressure-temperature of metamorphism within

51 it are similar to that of continent-continent collision within the Himalayan orogen (Weller
 52 & St-Onge, 2017). The terminal closure of the intervening ocean basin between the Su-
 53 perior and composite Slave + Hearne + Rae provinces is interpreted in paleogeographic
 54 models to be associated not only with the assembly of Laurentia, but also with the con-
 55 joining of other continents into the hypothesized supercontinent Nuna (Pehrsson et al.,
 56 2015).

57 The rapid Paleoproterozoic amalgamation of the Laurentia craton led to the large
 58 persistent area of continental lithosphere that would grow further through accretionary
 59 orogenesis subsequently in the Paleoproterozoic Era and through the Mesoproterozoic
 60 Era (Whitmeyer & Karlstrom, 2007). This subsequent orogenesis along the southern to
 61 eastern margin of Laurentia (present-day coordinates) indicates that it was a long-lived
 62 accretionary margin (Karlstrom et al., 2001; Whitmeyer & Karlstrom, 2007). This ac-
 63 cretionary margin has been interpreted to have extended beyond Laurentia and have con-
 64 tinued onto Baltica and Australia (Karlstrom et al., 2001). Based on correlation of Archean
 65 provinces and Paleoproterozoic orogenic belts, Gower et al. (1990) reconstructed Baltica
 66 to Laurentia in a position known as the NENA (northern Europe and North America)
 67 configuration. This reconstruction is compatible with existing paleomagnetic constraints
 68 from *ca.* 1750 to 1270 Ma (Evans & Pisarevsky, 2008) and these conjoined cratons fea-
 69 ture as a major component of the hypothesized Nuna supercontinent (Evans & Mitchell,
 70 2011; Zhang et al., 2012).

71 Additional data that constrain the paleogeographic position of Laurentia from the
 72 time just following the Trans-Hudson orogeny can test the hypothesis of the unity of Lau-
 73 rentia's Archean provinces, establish the position of the newly amalgamated Laurentia,
 74 and thereby enable tests of hypothesized connections with other cratons. This study de-
 75 velops a new paleomagnetic pole for Laurentia from *ca.* 1780 Ma diabase dikes of the
 76 East-Central Minnesota Batholith (ECMB) that provides such constraints.

77 2 Geologic Setting

78 Coeval with collisional orogenesis between the assembling Archean provinces that
 79 formed Laurentia's core was the *ca.* 1860 to 1820 Ma accretionary Penokean orogeny along
 80 the southern margin of the Superior Province (Fig. 1; Schulz and Cannon (2007)). Penokean
 81 orogenesis resulted from island-arc and microcontinent collisions with the Superior Province

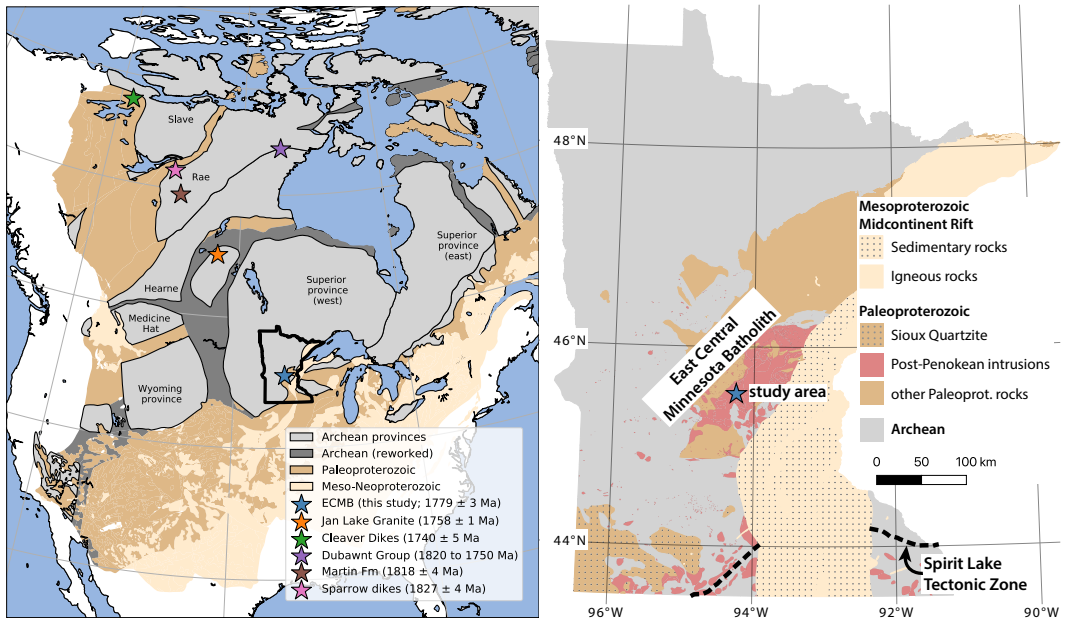


Figure 1. Map of Laurentia showing the location of Archean provinces and younger Proterozoic crust (simplified from Whitmeyer and Karlstrom (2007)). The localities of paleomagnetic poles that constrain Laurentia's position just after its amalgamation are shown with stars including the new pole from this study developed from the East-Central Minnesota Batholith (ECMB). The outline of the state of Minnesota around the ECMB blue star is the region for the geologic map in the right panel. This map shows interpreted Precambrian geology for the state of Minnesota (simplified from Jirsa et al. (2012)) including in regions covered by Phanerozoic sedimentary rocks where the Precambrian bedrock is inferred from geophysical data and drill cores.

82 that led to metamorphism of Superior Province lithologies and development of a fore-
 83 land basin (Schulz & Cannon, 2007; Holm et al., 2019). Following the Penokean orogeny,
 84 there was voluminous magmatism along the southeastern margin of the west Superior
 85 Province resulting in the emplacement of the *ca.* 1780 Ma East-Central Minnesota Batholith
 86 (ECMB) and other coeval post-orogenic plutons (Fig. 1; Holm et al. (2005); Boerboom
 87 et al. (2005); Schmitz et al. (2018)). While the ECMB is dominantly comprised of felsic
 88 to intermediate plutons, mafic magmas were also generated and commingled with the
 89 more abundant felsic magmas throughout the interval of batholith generation as evidenced
 90 by mafic enclaves within some of the plutons (Boerboom et al., 2005, 2011; Schmitz et
 91 al., 2018). Mafic melt within the ECMB also led to the emplacement of a set of near-
 92 vertical northeast-trending diabase dikes (Fig. 2; Boerboom et al. (2005)). The dikes have
 93 chilled margins and are typically 1 to 3 meters wide with widths up to 8 meters (Boerboom
 94 et al., 2005). As with the granites they intrude, the dikes have primary igneous texture

95 and no metamorphic fabric (Boerboom et al., 2005). They have experienced variable low-
96 grade alteration such as albitionization and sericitization of plagioclase and the formation
97 of pyrrhotite. These diabase dikes are present within all of the granitoid units of the ECMB
98 (e.g., St. Cloud Granite, Rockville Granite, and Reformatory Granodiorite; Fig. 2) with
99 the exception of the youngest Richmond Granite. Throughout the field area, the dikes
100 are exposed both in glacially-polished pavement outcrops and in numerous inactive and
101 active dimension stone granite quarries. Northeast-trending diabase dikes are present
102 in all of the quarries in the Rockville Granite, St. Cloud Granite as well as in the Re-
103 formatory granodiorite, regardless of the size of the quarry, as well as in many natural
104 bedrock outcrops. In many of the old inactive quarries, the north and/or south quarry
105 walls are marked by the planar surface of a diabase dike contact, where the rock nat-
106 urally separates, often resulting in elongated northeast-southwest shapes to the quarry
107 pits. In contrast, no diabase dikes have been found in the quarries or natural exposures
108 of the Richmond granite. Although this granite does not contain as many quarries and
109 there are fewer natural outcrops, the lack of diabase dikes contrasts sharply with the nu-
110 merous dikes present in the other nearby granites, where an equivalent exposed surface
111 area would contain numerous diabase dikes. This absence indicates that the younger Rich-
112 mond Granite post-dates the intrusion of the diabase dikes into the St. Cloud Granite,
113 Rockville Granite, and Reformatory Granodiorite.

114 There are also quartz-feldspar porphyry dikes with the same northeast-trending di-
115 rection as the diabase dikes found in all the granitoids also with the exception of the Rich-
116 mond Granite (Boerboom et al., 2005). These porphyritic microgranite dikes have chilled,
117 and locally flow-banded, margins. One has been observed to have intruded into a northeast-
118 trending diabase dike and another has textures consistent with commingling of magmas
119 between the felsic dike and adjacent diabase dike indicative of synchronous emplacement
120 (Boerboom & Holm, 2000). The Richmond Granite has trachytoid magmatic fabric de-
121 fined by aligned potassium-feldspar phenocrysts that share the same orientation with
122 the northeast-trending dikes (Boerboom & Holm, 2000), indicating that this orientation
123 is associated with a persistent regional stress field throughout the interval of magma em-
124 placement and dike formation. These field relationships indicate that the quartz-feldspar
125 porphyry and diabase dikes are comagmatic with the batholith. The diabase dikes are
126 constrained to be younger than the St. Cloud Granite (new U-Pb date of 1781.44 ± 0.51
127 Ma; 2σ analytical uncertainty) which they pervasively intrude, older than the Richmond

128 Granite (new U-Pb date of 1776.76 ± 0.49 Ma) in which they are absent, and similar
 129 in age to the quartz-feldspar porphyry dikes (new U-Pb date of 1780.78 ± 0.45 Ma).

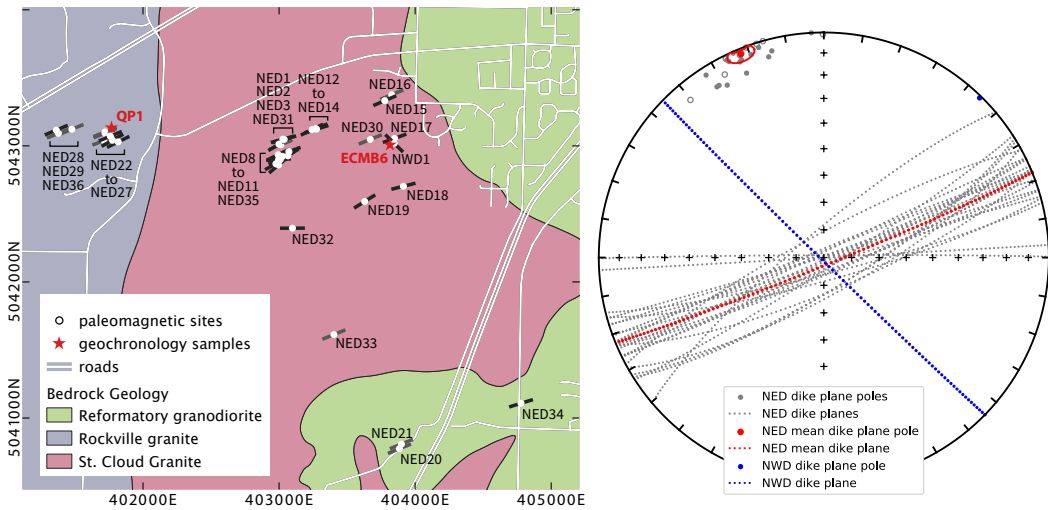


Figure 2. Left panel: Locations of paleomagnetic sites of the northeast-trending dikes (NED) and a northwest-trending dike (NWD) within the Rockville Granite, Reformatory Granodiorite and St. Cloud Granite of the ECMB (bedrock geology from Boerboom et al. (1995) and shown in UTM zone 15N WGS 84 coordinate reference system such that each axis tick is 1 km). Within regions of the mapped St. Cloud Granite there is more complex interfingering of that granite with the Reformatory Granodiorite than is shown. The strikes of the dikes are shown as lines (black when measured on that dike; grey when using the overall mean orientation from the measured NED dikes). The location of the QP1 and ECMB6 geochronology samples are shown. The ECMB4 geochronology sample was collected ~ 18 km SW of the western edge of the map, in the Richmond Granite which cross-cuts the Rockville Granite and is younger than the NED dikes. Right panel: The orientations of dikes. Each individual dike orientation is the mean of multiple measurements on that dike. The mean of the poles to the NED planes is shown with a red dot and a 95% confidence ellipse on the mean calculated with Fisher statistics. This confidence ellipse intersects the equator indicating that the mean plane cannot be distinguished from vertical.

130 3 Paleomagnetic Methods and Results

131 Oriented samples for paleomagnetism were collected and analyzed from 36 of the
 132 northeast-trending dikes of the ECMB and one northwest-trending dike (Fig. 2). Each
 133 sampled dike constituted a paleomagnetic site in our site naming scheme. These sites
 134 were concentrated in and around Stearns County Quarry Park near the city of St. Cloud
 135 (Fig. 2). Samples were collected from the dikes with a gas-powered drill and oriented
 136 in the field with a Pomeroy orienting fixture. The azimuthal orientations of the cores were
 137 determined either through sun or magnetic compass depending on cloud cover. Sun com-

138 pass directions were preferentially used when available. When magnetic compass data
139 were used they were corrected for local magnetic declination using the International Ge-
140 omagnetic Reference Field model (Thébault et al., 2015). Specimens from the oriented
141 samples were analyzed in the UC Berkeley Paleomagnetism lab using a 2G DC-SQUID
142 magnetometer. Samples either underwent stepwise alternating field (AF) or thermal de-
143 magnetization. Thermal demagnetization was accomplished using an ASC thermal de-
144 magnetizer (residual fields <10 nT). AF demagnetization was conducted with inline coils
145 that utilize a Crest Amplifier paired with an Adwin controller to develop a well-controlled
146 waveform. All paleomagnetic data developed in this study are available at the measure-
147 ment level in the MagIC database (<https://www.earthref.org/MagIC/> doi/ INSERT-
148 DOI; UPDATE TO DOI WHEN ASSIGNED).

149 Typical behaviors of sample remanence during demagnetization are illustrated for
150 representative specimens in Figure 3. AF demagnetization data typically reveal three
151 components: a small low-coercivity component approximately aligned with Earth's present
152 local field in the study region that was typically removed below 10 mT; a medium-coercivity
153 component that is steep and was dominantly removed between 10 and 60 mT; and a high-
154 coercivity component that was subsequently removed incompletely as demagnetization
155 progressed to 130 mT. These components are present to varying degrees within individ-
156 ual specimens (Fig. 3).

157 Sister specimens from some samples underwent thermal and AF demagnetization
158 which provides additional insight into the carriers of the components through compar-
159 ison of the thermal and AF demagnetization spectra (such as NED2-8 in Fig. 3). These
160 data reveal that the low-coercivity component direction is removed at the lowest unblock-
161 ing temperatures up to 150°C. This behavior, as well as the typical direction, is most con-
162 sistent with the component being a viscous overprint acquired in Earth's geomagnetic
163 field. The direction of the high-coercivity component is removed through thermal de-
164 magnetization between 250°C and 350°C — consistent with it being held by monoclinic
165 pyrrhotite. The direction of this magnetization held by pyrrhotite is aligned with the magnetite-
166 held remanence within a northwest-trending dike in the region (discussed in more de-
167 tail below) — a direction consistent with the position of Laurentia during the time pe-
168 riod of *ca.* 1096 Ma Midcontinent Rift magmatism (Swanson-Hysell et al., 2020). We
169 interpret this high-coercivity component held by pyrrhotite, whose presence is variable
170 in ECMB dikes, to have formed through hydrothermal activity associated with Midcon-

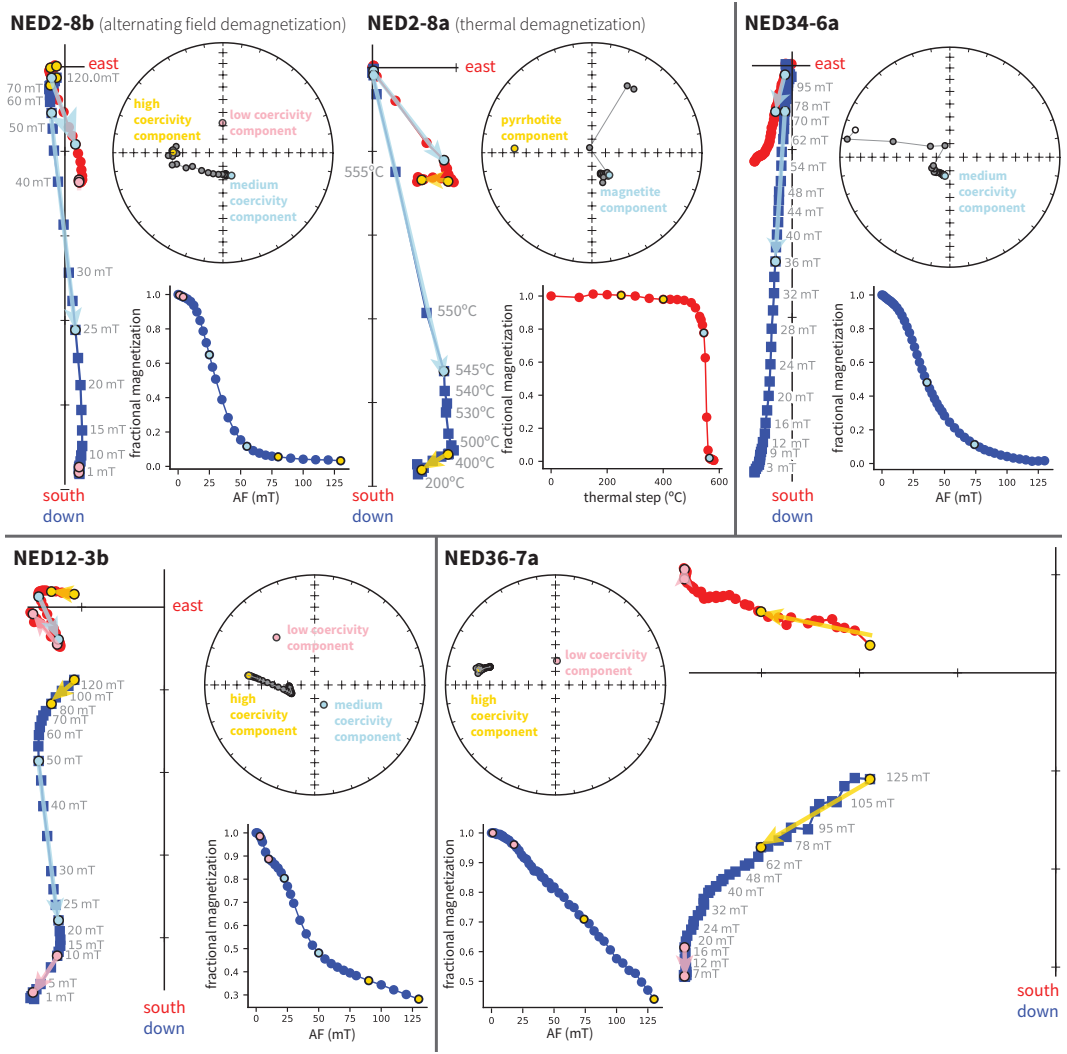


Figure 3. Paleomagnetic data from ECMB northeast-trending diabase dikes are shown in geographic coordinates on vector component plots, measurement-level equal area plots and magnetization magnitude plots (developed using PmagPy software; Tauxe et al. (2016)). Least-squares fits to the data are shown with colored arrows on the vector component plots, colored directions on the equal area plots, and as colored end-points on the magnetization magnitude plots (pink for low-coercivity; blue for medium-coercivity; yellow for high-coercivity). Specimens NED2-8a and NED2-8b are from the same core sample and were analyzed via thermal and alternating field (AF) demagnetization respectively. These data from sample NED2-8 reveal the steep medium-coercivity component to thermally unblock at temperatures characteristic of remanence held by magnetite and the high-coercivity component to thermally unblock at temperatures characteristic of pyrrhotite. Specimen NED34-6a is dominated by the steep medium-coercivity component. The medium-coercivity component is well-resolved in specimen NED12-3b which also has a substantial high-coercivity component. The high-coercivity component dominates the remanence of specimen NED36-7a such that no medium-coercivity component can be resolved.

171 tinent Rift magmatism such as that represented by the emplacement of the northwest-
 172 trending dike. The pyrrhotite thereby carries a chemical remanent magnetization.

173 In some specimens, the low-coercivity component is much larger and has a direc-
 174 tion that is distinct from the present local field. It is likely that these samples acquired
 175 an isothermal remanent magnetization associated with quarrying operations or lightning
 176 strikes. This behavior can be prevalent throughout a site or can be present in just some
 177 samples from a given site. In many cases, these low-coercivity overprints can be removed
 178 through AF demagnetization and the medium-coercivity and/or high-coercivity compo-
 179 nents can be subsequently isolated. In some instances, however, these large and dom-
 180 inantly low-coercivity overprints extend to higher coercivities preventing the isolation
 181 of other components.

182 The medium-coercivity component direction is dominantly removed through ther-
 183 mal demagnetization between 515°C and 565°C consistent with it being held by low-Ti
 184 titanomagnetite. This direction was recovered with site mean direction uncertainty less
 185 than 8 degrees ($\alpha_{95} < 8^\circ$) for 23 sites (Table 1). We interpret this component to be a
 186 primary thermal remanence acquired at the time of dike emplacement as part of the *ca.*
 187 1780 Ma ECMB. This interpretation gains support from the rock magnetic data, an in-
 188 verse baked contact test, and thermochronology data that support an emplacement tem-
 189 perature well below the blocking temperature of magnetite and a mild subsequent ther-
 190 mal history — as discussed in more detail below.

191 3.1 Magnetic mineralogy constraints from low-temperature magnetom- 192 etry

193 To gain additional insight into the magnetic mineralogy of the dikes, a Magnetic
 194 Properties Measurement System (MPMS) at the Institute for Rock Magnetism was used
 195 to conduct low-temperature remanence experiments. In the field-cooled (FC) experiments
 196 shown in Figure 4, the magnetization was measured upon warming following the spec-
 197 imen having cooled in an applied field of 2.5 T from 300 to 10 K. In the zero-field-cooled
 198 (ZFC) experiment, a low-temperature saturation isothermal remanence (LTSIRM) of 2.5
 199 T was applied at 10 K after the specimen cooled in a (near-)zero field. In the room-temperature
 200 saturation isothermal remanence (RTSIRM) experiment, the sample was pulsed with a
 201 2.5 T field at room temperature (~ 300 K) and then cooled to 10 K and warmed back

to room temperature in a (near-)zero field. These experiments reveal that sister specimens to paleomagnetic specimens whose remanence is dominated by the medium-coercivity component without an appreciable high-coercivity component have strong expressions of the ~ 120 K Verwey transition as expected for a ferromagnetic mineralogy of well-preserved low-Ti titanomagnetite (NED34-6c in Fig. 4; Verwey (1939); Feinberg et al. (2015)). In contrast, specimens from samples that have a larger contribution of the high-coercivity component have weaker saturation magnetization, minor expression of the Verwey transition, and the presence of monoclinic pyrrhotite as evidenced through the ~ 30 K Besnus transition (NED36-8c in Fig. 4; Besnus and Meyer (1964); Feinberg et al. (2015)). Samples with a smaller contribution of the high-coercivity component superimposed on the medium-coercivity component have intermediate behavior with a minor expression of the Besnus transition and a more prominent Verwey transition (NED2-8c in Fig. 4). These results support the interpretation that the medium-coercivity component is held by primary unaltered (titano)magnetite and that the high-coercivity component is the result of subsequent alteration that resulted in degradation of magnetite and formation of pyrrhotite.

217 3.2 Baked contact test

One northwest-trending dike is exposed and was sampled within the study region as site NWD1 (Fig. 2). The magnetization direction of this dike indicates that it is associated with the main stage of the Midcontinent Rift (*ca.* 1096 Ma) as it has a normal polarity and an inclination consistent with that time interval of Midcontinent Rift volcanism (Fig. 5; Swanson-Hysell et al. (2020)). The dike cross-cuts one of the northeast-trending dikes (NED17) allowing for a baked contact test (Figs. 2 and 5). The baked contact test is positive with a distinct direction in the northeast-trending dike (corresponding to the remanence direction seen throughout the northeast-trending dikes of the ECMB) with its magnetite remanence becoming progressively overprinted by the northwest-trending dike up to the contact (Fig. 5). This positive baked contact test indicates that the northeast-trending ECMB dikes have not been overprinted since the northwest-trending dike was emplaced (*ca.* 1096 Ma). This positive baked contact test for the northwest-trending dike constitutes what is referred to as a positive “inverse” baked contact test for the northeast-trending dike remanence — it constrains the remanence to be more ancient than the *ca.* 1.1 Ga Mesoproterozoic northwest-trending dike, but does not provide a constraint back to the Paleoproterozoic time of dike emplacement. Given that the

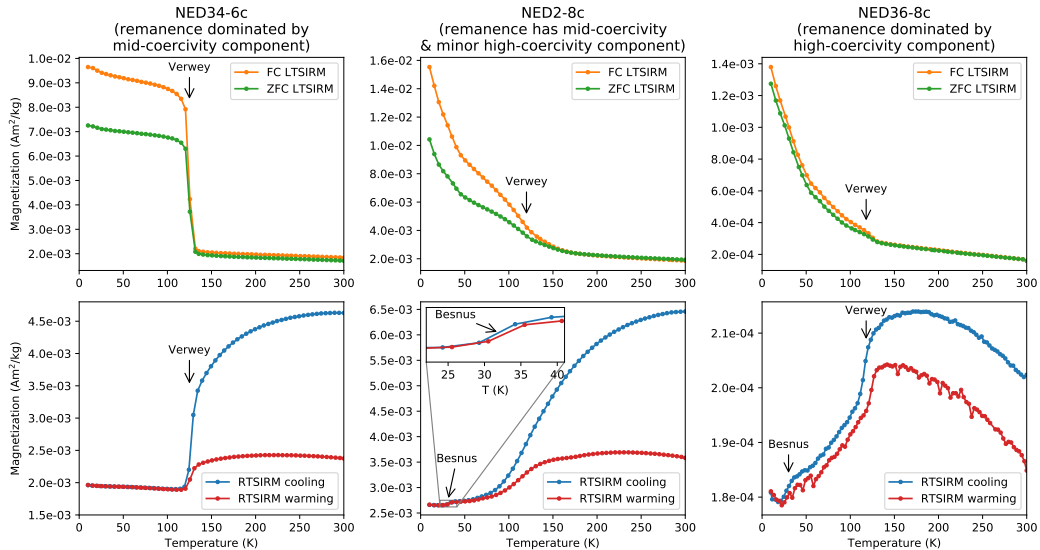


Figure 4. Low-temperature remanence experiment data. The specimen from a sample whose natural remanent magnetization is dominated by the medium-coercivity component (NED34-6c) has behavior dominated by magnetite as evidenced through the response across the ~ 120 K Verwey transition. The specimen from a sample whose natural remanence is dominated by the high-coercivity component (NED36-8c) has weaker magnetization, a relatively minor expression of the Verwey transition, and expression of the ~ 32 K Besnus transition that indicates the presence of monoclinic pyrrhotite. The specimen whose natural remanence has a well-resolved medium-coercivity component with a minor high-coercivity component (NED2-8c) has intermediate behavior with a Verwey transition that is not as suppressed as in NED36-8c with a minor, but resolvable, Besnus transition (see inset). FC: field-cooled; ZFC: zero-field-cooled; LTSIRM: low-temperature saturation isothermal remanence magnetization; RTSIRM: room-temperature saturation isothermal remanence magnetization.

host rocks for the northeast-trending dikes are of a very similar age to the dikes themselves there is not the possibility of a Paleoproterozoic baked contact test. In contrast to the dikes, stable and consistent remanence directions were not recovered from pilot sites in ECMB granites.

The high-coercivity remanence direction held by pyrrhotite in some of the northeast-trending dikes is aligned with the remanence direction of the northwest-trending dike. While the thermal effect of the northwest-trending dike was limited to a few meters on either side of it as evidenced through the baked contact test (Fig. 5), there was more widespread hydrothermal alteration associated with Midcontinent Rift magmatic activity that led to the formation of pyrrhotite and an associated chemical remanent magnetization. In the majority of the northeast-trending dikes, the original magnetite is well-preserved (e.g., NED34 of Figs. 3 and 4) while other dikes experienced variable magnetite

alteration and the formation of secondary pyrrhotite (e.g., NED36 of Figs. 3 and 4). These components can be separated through progressive demagnetization (e.g., NED12 of Figs. 3) enabling the thermal remanent magnetization held by magnetite to be used to determine site mean directions and calculate a paleomagnetic pole (Fig. 6).

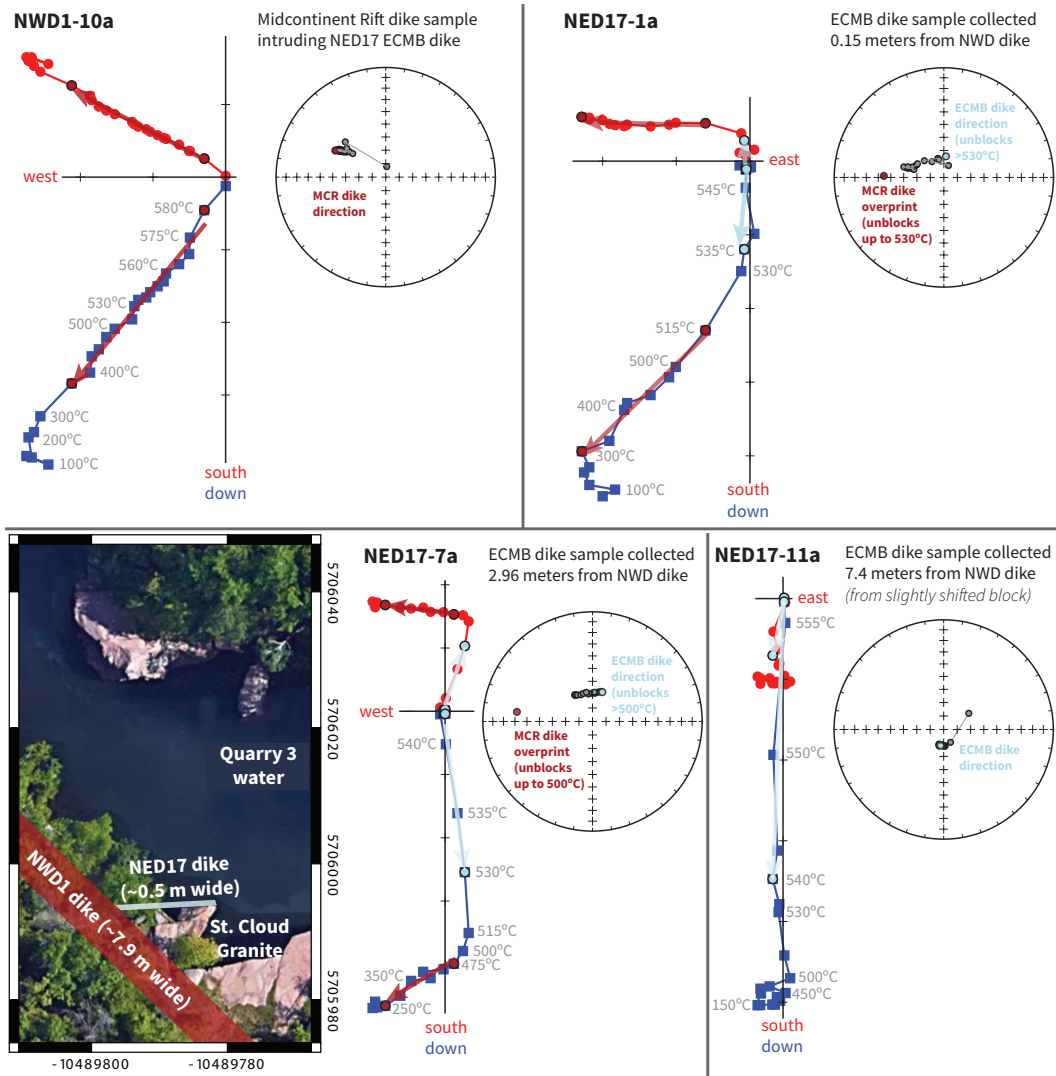


Figure 5. Results from a positive baked contact test where a northwest-trending dike (site NWD1) cross-cuts a northeast-trending dike (site NED17). The NWD1 dike has a direction indicating that it formed during the *ca.* 1096 Ma main stage of rift volcanism. Close to the NWD1 dike the NED17 is nearly fully overprinted (NED17-1a). Further from NWD1 there are partial thermal overprints (NED17-7a) that by ~7 meters from the cross-cutting dike are not resolvable (NED17-11a). Note that blocks from this dike were slightly shifted due to quarrying operations which does not bear on the significance of the positive test, but has led to the exclusion of the result from the site mean compilation and overall pole.

250 **3.3 Paleomagnetic pole**

251 The site mean directions determined from the magnetite remanence component can
 252 be converted to virtual geomagnetic poles and then used to calculate a mean paleomag-
 253 netic pole for the ECMB diabase dikes (pole longitude: 265.8° ; pole latitude: 20.4° ; A_{95} :
 254 4.5° ; K: 45.6 N: 23 ; Fig. 6). These 23 virtual geomagnetic poles have a distribution con-
 255 sistent with a Fisher distribution as determined through the Fisher et al. (1987) goodness-
 256 of-fit method. The A_{95} uncertainty on the mean pole position of 4.5° is within the bounds
 257 of reliability proposed by Deenen et al. (2011). It is well below the A_{95} -max value pro-
 258 posed to establish a well-determined mean for 23 sites (11.4°) and above the A_{95} -min
 259 value (3.4°) consistent with the site directions having sufficiently sampled secular vari-
 260 ation of the geomagnetic field.

261 In a massive host rock such as the ECMB plutons without preferential bedding or
 262 foliation, it is expected that lithospheric stresses will lead to the emplacement of near
 263 vertical dikes. Dike plane orientations were measured on each dike for which there was
 264 sufficient three-dimensional exposure. Multiple measurements were made for each dike
 265 to constrain their orientation. The mean strike calculated from 17 dike orientations is
 266 067° and the mean dip is 88° (Fig. 2). The α_{95} uncertainty associated with the Fisher
 267 mean for the poles to these dike orientation planes (i.e. the lines perpendicular to the
 268 planes) is 4.7° which means that the overall orientation of the planes is statistically in-
 269 distinguishable from vertical (Fig. 2). Due to this verticality, we interpret the exhumation
 270 of the ECMB plutons to have not resulted in appreciable tilting since dike emplace-
 271 ment and do not apply a tilt correction to the paleomagnetic data.

272 **4 Geochronology Methods and Results**

273 The field relationships show the diabase dikes to be younger than the Rockville Gran-
 274 ite, Reformatory Granodiorite and the St. Cloud Granite which they pervasively intrude
 275 and to be older than the Richmond Granite where they are absent (Boerboom et al., 2005).
 276 Holm et al. (2005) developed U-Pb dates calculated as concordia intercept dates from
 277 these intrusions. The dates reported by Holm et al. (2005) for granites intruded by the
 278 dikes are 1783 ± 11 Ma for the Reformatory Granodiorite, 1780 ± 7 Ma for the Rockville
 279 Granite and 1779 ± 5 Ma for the St. Cloud Granite. The younger cross-cutting Rich-
 280 mond Granite has a date of 1772 ± 3 Ma (Holm et al., 2005). An age of 1774 ± 7 Ma

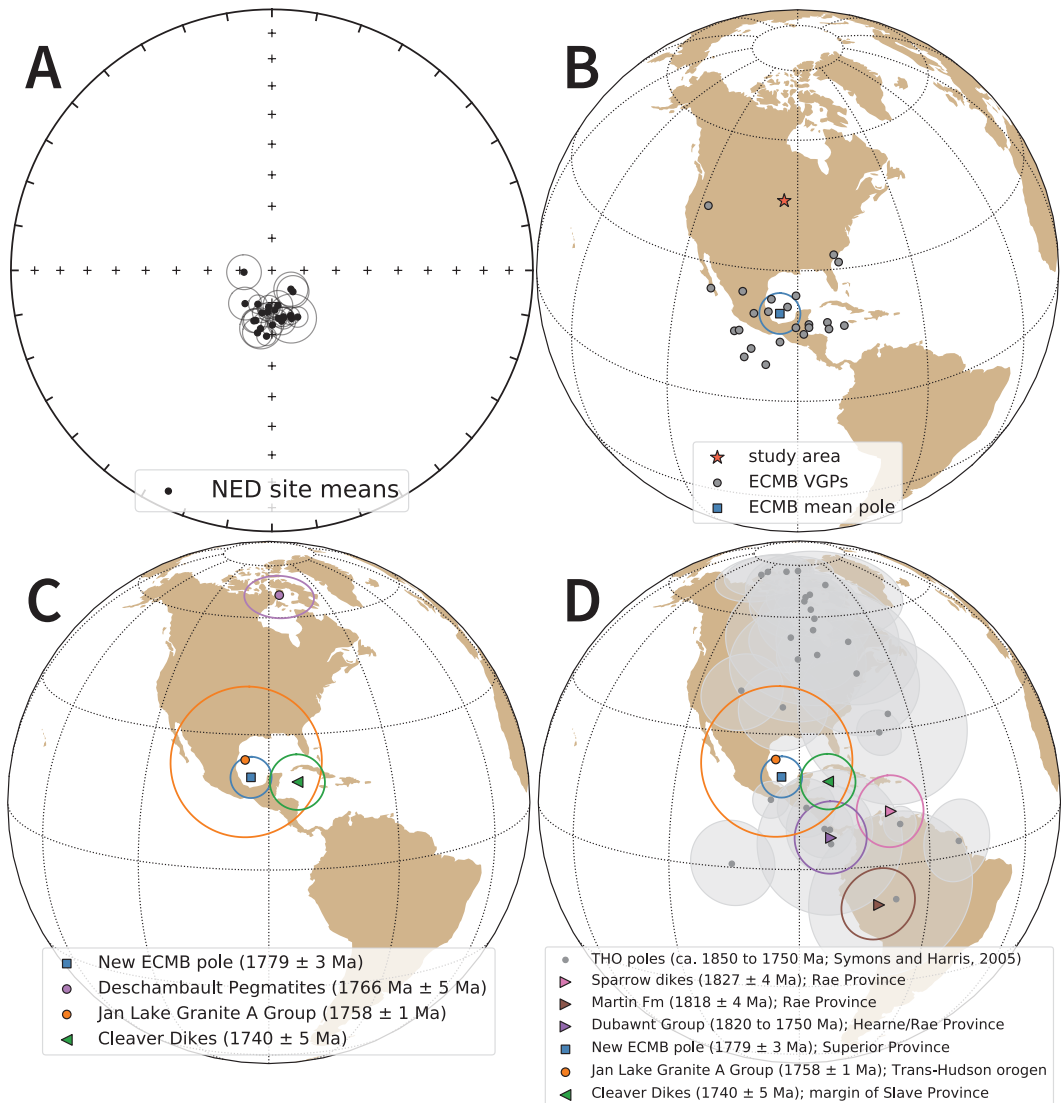


Figure 6. A) Site mean directions for the magnetite remanence of the northeast-trending (NED) ECMB diabase dikes with $\alpha_{95} < 8^\circ$. B) Virtual geomagnetic poles (VGPs) calculated from these site means and the overall mean paleomagnetic pole for the ECMB dikes. C) Comparison between the new ECMB paleomagnetic pole and other *ca.* 1780 to 1740 Ma poles for Laurentia. D) Comparison of poles from Laurentia's provinces from 1830 to 1740 Ma from Evans et al. (2021) as well as poles from the Trans-Hudson orogen (THO; grey; Symons and Harris (2005)) with the new ECMB pole.

for one of the quartz-feldspar porphyry dikes developed by Holm et al. (2005) is consistent with this interpretation of these dikes being older than the Richmond Granite (and younger than the granites they intrude). While the dates published in Holm et al. (2005) are valuable constraints and are consistent with the field relationships, they are of lower precision than what is possible with modern analytical approaches and therefore lead

286 to overlapping uncertainties. Higher precision constraints resulting from methods that
 287 apply ion-exchange separation with low blank analyses of chemically-abraded single zir-
 288 con grains can test the field relationship interpretations and provide more confidence in
 289 the overall age constraints.

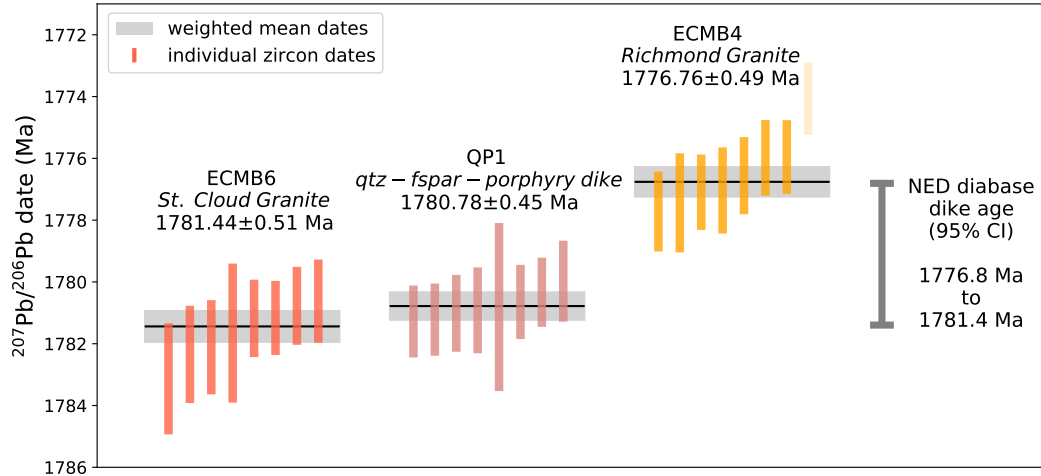


Figure 7. U-Pb dates for ECMB samples. Weighted mean dates (horizontal lines) are calculated from individual zircon dates (vertical bars). The NED diabase dikes intrude the St. Cloud Granite such that the ECMB6 weighted mean date of 1781.44 ± 0.51 Ma is a maximum age. The quartz-feldspar porphyry dikes (one of which was sampled as QP1) also intrude the St. Cloud Granite and are parallel to the NED diabase dikes. Neither the quartz-porphyry dikes nor the diabase dikes intrude the younger cross-cutting Richmond Granite such that the ECMB4 weighted mean date of 1776.76 ± 0.49 Ma provides a minimum age for the dikes. Details for the weighted mean dates are given in Table 2 and individual zircon data are in the Supporting Information.

290 To further constrain the age of the northeast-trending diabase dikes, we developed
 291 new isotope dilution-thermal ionization mass spectrometry (ID-TIMS) U-Pb zircon dates
 292 from the St. Cloud Granite that host the dikes (sample ECMB6), the Richmond Gran-
 293 ite from which the dikes are absent (sample ECMB4), and from a northeast-trending quartz-
 294 feldspar porphyry dike (sample QP1) that is likely coeval with the diabase dikes (Figs.
 295 2 and 7). Zircon crystals were chemically abraded prior to analysis of single zircon grains
 296 by ID-TIMS at the Boise State Isotope Geology Laboratory (detailed geochronology meth-
 297 ods are provided in the Supporting Information). Weighted mean dates were calculated
 298 from multiple single zircon dates (Fig. 7; Table 2). While chemical abrasion served to
 299 reduce Pb-loss and resulted in concordant analyses, some grains have persistent Pb-loss
 300 and are discordant (Fig. S1). As a result, we calculate weighted mean $^{207}\text{Pb}/^{206}\text{Pb}$ dates
 301 rather than $^{206}\text{Pb}/^{238}\text{U}$ dates (Fig. 7; Table 2). These $^{207}\text{Pb}/^{206}\text{Pb}$ dates are 1781.44

302 ± 0.51 Ma (2σ analytical uncertainty; MSWD = 1.24; n=8) for the St. Cloud Granite
 303 (ECMB6) and 1776.76 ± 0.49 Ma (MSWD = 1.15; n=7) for the Richmond Granite (ECMB4;
 304 Fig. 7). The date for the sampled quartz-feldspar porphyry dike (QP1) of 1780.78 ± 0.45
 305 Ma (MSWD = 0.53; n=8) is between these two dates as expected on the basis of field
 306 relationships. Taking into account the analytical uncertainty on the maximum and min-
 307 imum age constraints, the diabase dikes are younger than the 1781.44 ± 0.51 Ma St. Cloud
 308 Granite and older than the 1776.76 ± 0.49 Ma Richmond Granite. If one assumes a uni-
 309 form probability of diabase emplacement timing between the maximum and minimum
 310 age constraints that have normally distributed uncertainties, the 95% confidence inter-
 311 val can be estimated through Monte Carlo simulation. Applying this approach gives a
 312 mean age of 1779.1 Ma with 95% confidence interval (CI) bounds of 1776.8 to 1781.4 Ma.
 313 We can succinctly state the age of the northeast-trending ECMB diabase dikes as be-
 314 ing 1779.1 ± 2.3 Ma (95% CI).

315 5 Thermochronology Methods and Results

316 While the U-Pb zircon dates constrain the crystallization ages of the ECMB in-
 317 trusions, additional insight into the thermal history of the batholith can help with in-
 318 terpretation of the paleomagnetic data given that the thermal remanent magnetization
 319 of magnetite will be blocked at temperatures below 580°C. As discussed below, existing
 320 Ar-Ar dates on hornblende and biotite from the ECMB provide valuable constraints in
 321 this regard (Fig. 8). In this study, we also develop new U-Pb apatite dates from three
 322 ECMB granites (ECMB1, the Isle Granite; ECMB3, the Rockville Granite; ECMB4, the
 323 Richmond Granite). In contrast to zircon, for which the temperatures of appreciable Pb
 324 diffusion exceed the liquidus of granite (Cherniak & Watson, 2001), the temperature win-
 325 dow for closure of the U-Pb system in apatite is much lower (~ 510 to 460 °C; Smye et
 326 al. (2018)). As a result, U-Pb dates of apatite serve as a thermochronometer at moderately-
 327 high temperatures (Chamberlain & Bowring, 2001; Schoene & Bowring, 2007; Cochrane
 328 et al., 2014). These temperatures are of particular relevance to the interpretation of the
 329 paleomagnetic data as they are lower than, or correspond with, the blocking tempera-
 330 ture of low-Ti titanomagnetite. If a pluton was emplaced at depths where temperatures
 331 exceed the closure temperature of apatite, or if it experienced prolonged reheating, the
 332 U-Pb apatite dates would be appreciably younger than the U-Pb zircon crystallization
 333 dates.

334 U-Pb data were developed from apatite grains separated from ECMB granites through
335 laser ablation inductively coupled plasma mass spectrometry (LA-ICP-MS) at UC Santa
336 Barbara (method details are provided in the supporting information). In contrast to zir-
337 con, apatite incorporates significant Pb at the time of crystallization. As a result of this
338 elevated common Pb, U-Pb dates were determined through the calculation of Tera-Wasserburg
339 concordia lower intercept dates where the upper intercept corresponds to the ratio of ini-
340 tial $^{207}\text{Pb}/^{206}\text{Pb}$ and the lower intercept is the $^{206}\text{Pb}/^{238}\text{U}$ date (following the method
341 of Ludwig (1998) as implemented in the IsoplotR software of Vermeesch (2018); Fig. S2).
342 Sample ECMB1 is from the Isle Granite which has a U-Pb zircon date of 1779 ± 26 Ma
343 (Holm et al., 2005). The U-Pb apatite date for ECMB1 is $1800.3 \pm 33.4/65.2$ Ma where
344 the first uncertainty is the 2σ analytical uncertainty and the second uncertainty is 95%
345 confidence interval for the date that incorporates overdispersion (this uncertainty scheme
346 will be used for all the presented apatite dates). This U-Pb apatite date is therefore in-
347 distinguishable from the U-Pb crystallization date (Fig. 8). Sample ECMB3 is from the
348 Rockville Granite which has a U-Pb zircon date of 1780 ± 7 Ma (Holm et al., 2005). The
349 U-Pb apatite date for ECMB3 is $1810.5 \pm 16.2/23.0$ Ma. The youngest end of the overdis-
350 perspersion uncertainty range is very similar to (albeit just slightly older than) the U-Pb zir-
351 con date. It is not geologically reasonable for the U-Pb apatite date to be older than the
352 U-Pb zircon date. This result therefore suggests that the U-Pb apatite date uncertainty
353 is a slight underestimate with the U-Pb apatite system having closed just after the time
354 of zircon crystallization as constrained through the U-Pb zircon date. Sample ECMB4
355 is from the Richmond Granite for which we have developed a new ID-TIMS U-Pb zir-
356 con date of 1776.76 ± 0.49 Ma. The U-Pb apatite date for ECMB4 is $1751.7 \pm 17.8/36.6$
357 Ma which is indistinguishable from the U-Pb zircon date (Fig. 8).

358 Pb closure temperatures (T_c) for the analyzed apatite grains can be estimated with
359 the Dodson (1973) approach assuming a cylindrical geometry with half-widths as the char-
360 acteristic diffusion length. Apatite grain sizes are similar across the three dated spec-
361 imens; they typically are 100-200 μm long and 50-75 μm wide. Using the Pb diffusiv-
362 ity values of Cherniak et al. (1991), a cooling rate of $20^\circ\text{C}/\text{Myr}$ results in closure tem-
363 peratures of 463°C to 473°C for these grain sizes. A more rapid cooling rate is likely for
364 the batholith given the similarity of the U-Pb apatite dates with the U-Pb zircon dates.
365 A cooling rate of $100^\circ\text{C}/\text{Myr}$ from crystallization to apatite closure temperatures results
366 in closure temperatures of 493°C to 505°C .

367 Overall, these data indicate that the samples cooled through the \sim 500°C closure
 368 temperatures of the U-Pb apatite system near the time of zircon crystallization consist-
 369 ent with rapid cooling rates of the plutons (Fig. 8). Additionally, there has not been
 370 significant diffusion due to later tectonothermal events. As discussed below, this result
 371 is consistent with Ar-Ar hornblende dates from the ECMB granites and supports the mag-
 372 netite remanence being a primary thermal remanent magnetization.

373 **6 Discussion**

374 **6.1 Thermal history of the ECMB and a primary interpretation of the**
 375 **ECMB dike pole**

376 Prior to the emplacement of the ECMB, Paleoproterozoic host rocks were meta-
 377 morphosed to amphibolite facies during the Penokean orogeny (Holm & Silverstone, 1990).
 378 Emplacement of the ECMB has been hypothesized to be post-orogenic and associated
 379 with an interval of extensional collapse of the orogen (Holm & Lux, 1996; Boerboom &
 380 Holm, 2000). The Al-in-hornblende igneous barometer was applied to the St. Cloud and
 381 Isle Granites of the ECMB by Holm, Darrah, and Lux (1998). This barometer has vary-
 382 ing published calibrations. Applying the pressure calibration of Mutch et al. (2016) to
 383 the data in Holm, Darrah, and Lux (1998) and assuming a 2.7 g/cm³ overburden gives
 384 an estimated emplacement depth of 10.8 ± 1.7 km for the Freedhem Granodiorite, \sim 10.4
 385 \pm 1.7 km for the Isle Granite and 13.4 ± 2.1 km for the St. Cloud Granite. The cali-
 386 bration of Ague (1997) leads to slightly higher calculated pressures implying depths that
 387 are \sim 2.3 km deeper.

388 Thermochronology data give additional insight into emplacement temperatures (and
 389 thereby depth). Both the Ar-Ar hornblende dates published by Holm et al. (2005) and
 390 the U-Pb apatite dates developed in this study from ECMB lithologies are indistin-
 391 guishable from the crystallization ages of the intrusions (Fig. 8). The closure temperature for
 392 Ar in hornblende is \sim 580 to 490°C (Harrison, 1982). The closure of the U-Pb system in
 393 the dated apatite grains is \sim 500 to 460°C. The consistency between the U-Pb zircon crys-
 394 tallization and the U-Pb apatite and Ar-Ar hornblende cooling dates indicates that the
 395 present-day erosion level of the ECMB was at a shallow enough depth that the crustal
 396 temperatures were lower than these closure temperatures at the time of emplacement
 397 of the plutons. Geothermal gradients in continental arc settings are typically between

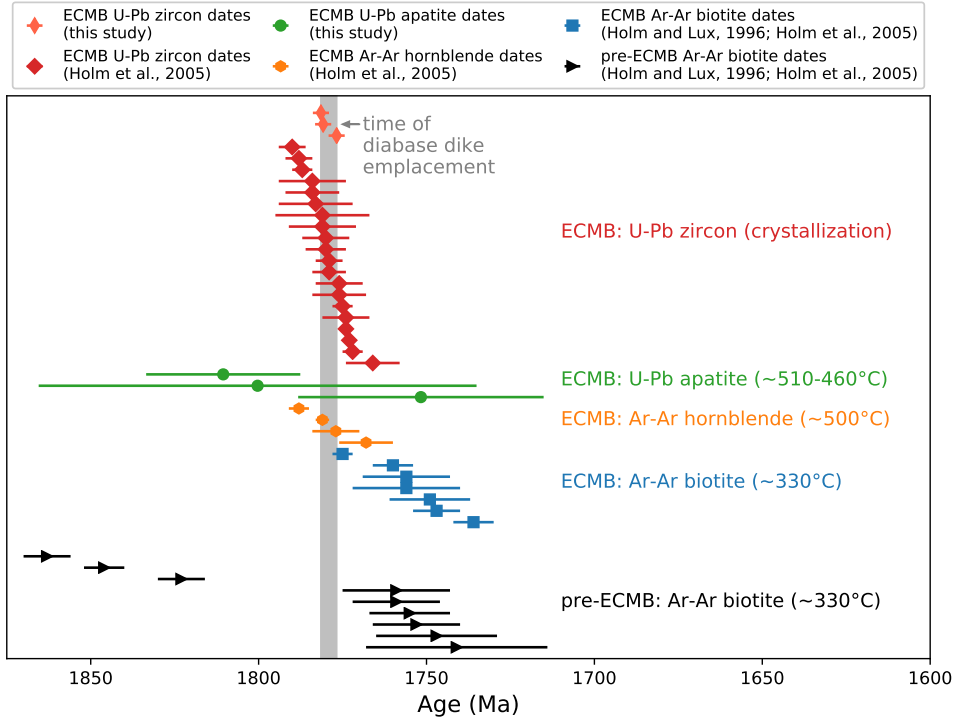


Figure 8. Summary of U-Pb zircon dates, U-Pb apatite dates, Ar-Ar hornblende, and Ar-Ar biotite dates from the East-Central Minnesota batholith (ECMB) from this study, Holm and Lux (1996) and Holm et al. (2005). Approximate closure temperatures associated with the thermochronometers are labeled next to the relevant data. That the U-Pb apatite and Ar-Ar hornblende dates are indistinguishable from the U-Pb zircon crystallization dates indicates that the plutons were emplaced at upper middle to upper crustal levels. The Ar-Ar biotite dates from both the ECMB plutons and older host rock lithologies indicate exhumation within \sim 20 million years to shallower depths and a lack of regional tectonothermal activity over the following 1.75 billion years.

398 25 to 45°C/km – potentially higher at 1.8 Ga (Rothstein & Manning, 2003). Taking a
 399 geothermal gradient of 30°C/km and the closure temperature constraints indicates that
 400 the plutons were emplaced at 15 km or shallower in the continental lithosphere. This
 401 emplacement depth is consistent with the Al-in-hornblende paleobarometry estimates.

402 Ar-Ar biotite dates provide insight into even lower temperatures as the system blocks
 403 at \sim 330°C (Grove & Harrison, 1996), well below the blocking temperature of magnetite
 404 magnetization in the dikes. Ar-Ar biotite dates from ECMB plutons range from over-
 405lapping the crystallization dates to being younger by \sim 20 million years (Fig. 8). Ar-Ar
 406 biotite dates from older host lithologies to the ECMB are either older than the age of
 407 the batholith itself or the same age as the Ar-Ar biotite dates from the batholith (Fig.

408 8). These data suggest that the batholith was emplaced near the upper depth range es-
409 timates from the Al-in-hornblende barometry (~ 10 km) and underwent exhumation to
410 below the $\sim 330^{\circ}\text{C}$ closure temperature of the K-Ar biotite system soon after emplace-
411 ment of the plutons. These data also indicate that there has not been reheating or per-
412 vasive fluid flow that would have perturbed the Ar-Ar thermochronometers in the gran-
413 ites in the time since initial cooling. The magnetization used to develop the paleomag-
414 netic pole comes from remanence held by low-Ti magnetite that dominantly unblocks
415 between 540 and 560°C (Figs. 3 and 5). The thermochronology results constrain the rocks
416 to have cooled through the magnetite blocking temperatures at the time that the dikes
417 were emplaced within the batholith and to not have experienced reheating that would
418 have perturbed the thermochronometers. These data support an interpretation that the
419 magnetite remanence within the ECMB dikes is a primary thermal remanent magneti-
420 zation.

421 These thermochronology data also demonstrate that following the emplacement of
422 the ECMB there were not regional tectonothermal events with the potential to have ther-
423 mally modified the magnetization of the magnetite within the ECMB diabase dikes. Sub-
424 sequent Paleoproterozoic Yavapai and Mazatzal accretion occurred to the southeast of
425 the Spirit Lake Tectonic zone on the other side of the Minnesota River Valley promon-
426 tory (~ 160 km south of the study region; Fig. 1; Holm et al. (2007)). In contrast to the
427 northeast-trending dikes in the ECMB, northeast-trending dikes in Wisconsin within *ca.*
428 1840 Ma plutons were metamorphosed to amphibolite facies associated with such accre-
429 tionary orogenesis (Holm et al., 2019). Mazatzal orogeny deformation and metamorphism
430 occurred *ca.* 1650 to 1630 Ma within the juvenile accreted island arc of the Wisconsin
431 Magmatic Terrane (Holm, Schneider, & Coath, 1998). The region of the ECMB was not
432 affected by these tectonothermal events (Fig. 1, Holm et al. (2005)). Holm et al. (2005)
433 proposed that the voluminous ECMB batholith stabilized the continental lithosphere and
434 prevented the region from being modified during subsequent collisions along the mar-
435 gin. This lack of deformation in the region of the ECMB is further supported by the nearly
436 horizontal bedding of *ca.* 1.63 Ga siliciclastic sedimentary rocks on either side of the batholith
437 (Holm, Schneider, & Coath, 1998; Medaris et al., 2021). In southwestern Minnesota, plu-
438 tons coeval with the ECMB are overlain by the subhorizontal Sioux Quartzite (Fig. 1)
439 with the correlative Barron Quartzite of northwestern Wisconsin also being undeformed
440 (Southwick et al., 1986). This lack of deformation contrasts with correlative Baraboo

quartzite south of the Spirit Lake Tectonic Zone (~400 km from the ECMB) that underwent compressional deformation during subsequent orogenesis (Holm, Schneider, & Coath, 1998; Medaris et al., 2021). The Yavapai and Mazatzal terranes were intruded by *ca.* 1470 to 1430 Ma granites of the Eastern Granite Rhyolite Province and there is a sizeable pluton of this age within accreted Penokean rocks in northern Wisconsin (the *ca.* 1470 Ma Wolf River batholith; Dewane and Van Schmus (2007)). However, the thermal effects of the Wolf River batholith (~370 km east of the ECMB study area) were limited to a 10-15 km wide contact zone surrounding the intrusion (Holm et al., 2019).

The one major subsequent tectonothermal event in the region for which there is localized evidence in the ECMB is the development of the Midcontinent Rift that initiated *ca.* 1109 Ma and in which magmatic activity continued to *ca.* 1084 Ma (Fig. 1; Fairchild et al. (2017); Swanson-Hysell et al. (2019)). While the main rift axis can be inferred from gravity and aeromagnetic anomaly data to be located ~75 km southeast of the study region (Fig. 1), the studied northwest-trending dike has a magnetization direction that implies that it was emplaced during Midcontinent Rift development *ca.* 1096 Ma (Fig. 5). The baked contact test between that dike (NWD1) and the northeast-trending dike that it cross-cuts (NED17), indicates that the thermal effect of the dike emplacement and the Midcontinent Rift in general was localized within the immediate vicinity of that dike (a few meters; Fig. 5). However, this Midcontinent Rift magmatic activity did result in local hydrothermal alteration as evidenced by magnetization held by monoclinic pyrrhotite that is variably present through the ECMB dikes and is in the same direction as the magnetization of the northwest-trending dike (Fig. 3). This chemical remanent magnetization held by monoclinic pyrrhotite likely formed at relatively low temperatures. Phase relationships in the Fe-S system developed through hydrothermal recrystallization experiments show monoclinic pyrrhotite to form at temperatures below 250°C and likely above 75°C (Kissin & Scott, 1982). While in some sites, this pyrrhotite-forming alteration obscured the primary thermal remanence held by magnetite (e.g., NED36 in Fig. 3), in the majority of sites the magnetite remanence direction can be well-resolved (e.g., NED2, NED12 and NED34 in Fig. 3). As a result, the paleomagnetic directions used to calculate the paleomagnetic pole shown in Figure 6 are held by (titano)magnetite that recorded a thermal remanent magnetization upon cooling of the diabase dikes. This evidence for variable late Mesoproterozoic hydrothermal alteration of the dikes provides an explanation for Ar-Ar data developed from two northeast-trending diabase dikes that

were reported in Boerboom and Holm (2000). These Ar-Ar data did not yield a plateau age, but give whole rock total gas dates that are late Mesoproterozoic in age. An interpretation that these whole rock total gas ages correspond with the age of emplacement is difficult to reconcile with the cogenetic relationship between the diabase dikes, the quartz-feldspar porphyry dikes and the ECMB granites. K-Ar whole-rock ages of 1570 to 1280 Ma from the dikes reported in Hanson (1968) and discussed in Horan et al. (1987) are attributed to partial resetting. The evidence for fluid flow that led to the formation of pyrrhotite *ca.* 1096 Ma supports the hypothesis put forward by Horan et al. (1987), as well as by Boerboom and Holm (2000), that there was Mesoproterozoic disruption of the K-Ar isotopic system in the dikes such that the Mesoproterozoic Ar-Ar dates are the result of alteration of dikes which are Paleoproterozoic in age. The field relationships indicating that the northeast-trending diabase dikes are comagmatic with ECMB granites is also consistent with whole rock Pb isotope data that reveal very similar arrays implying a *ca.* 1.8 Ga isochron age for both lithologies (Horan et al., 1987).

Overall, the constraints requiring that the ECMB granites were emplaced at depths where the ambient temperature was below the closure of U-Pb apatite and Ar-Ar hornblende systems indicate that the comagmatic diabase dikes would have acquired their magnetization at the time of emplacement. The lack of significant thermal events that could have reset the magnetite magnetization is indicated by the geologic setting, the thermochronology data (including the Paleoproterozoic Ar-Ar biotite dates), and the positive inverse baked contact test. We therefore interpret the pole calculated from the magnetite remanence of the ECMB diabase dikes as a high-quality constraint on the paleogeographic position of Laurentia at the time the dikes intruded (1779.1 ± 2.3 Ma). The ECMB diabase dikes pole meets six of the seven criteria for the quality criteria Van der Voo (1990) and the Meert et al. (2020) reliability criteria with the only one not satisfied being due to the lack of dual polarity directions. This single polarity normal polarity is consistent with the polarity of the Cleaver Dykes and the proposal of Irving (2004) that there was a normal geomagnetic superchron that followed the Trans-Hudson orogeny.

502 6.2 Laurentia's paleomagnetic poles following the Trans-Hudson orogeny

The Trans-Hudson orogeny is a major event in the formation of Laurentia resulting from collision between the Superior province and the Churchill plate consisting of the composite Slave + Rae + Hearne provinces (Hoffman, 1988; Corrigan et al., 2009;

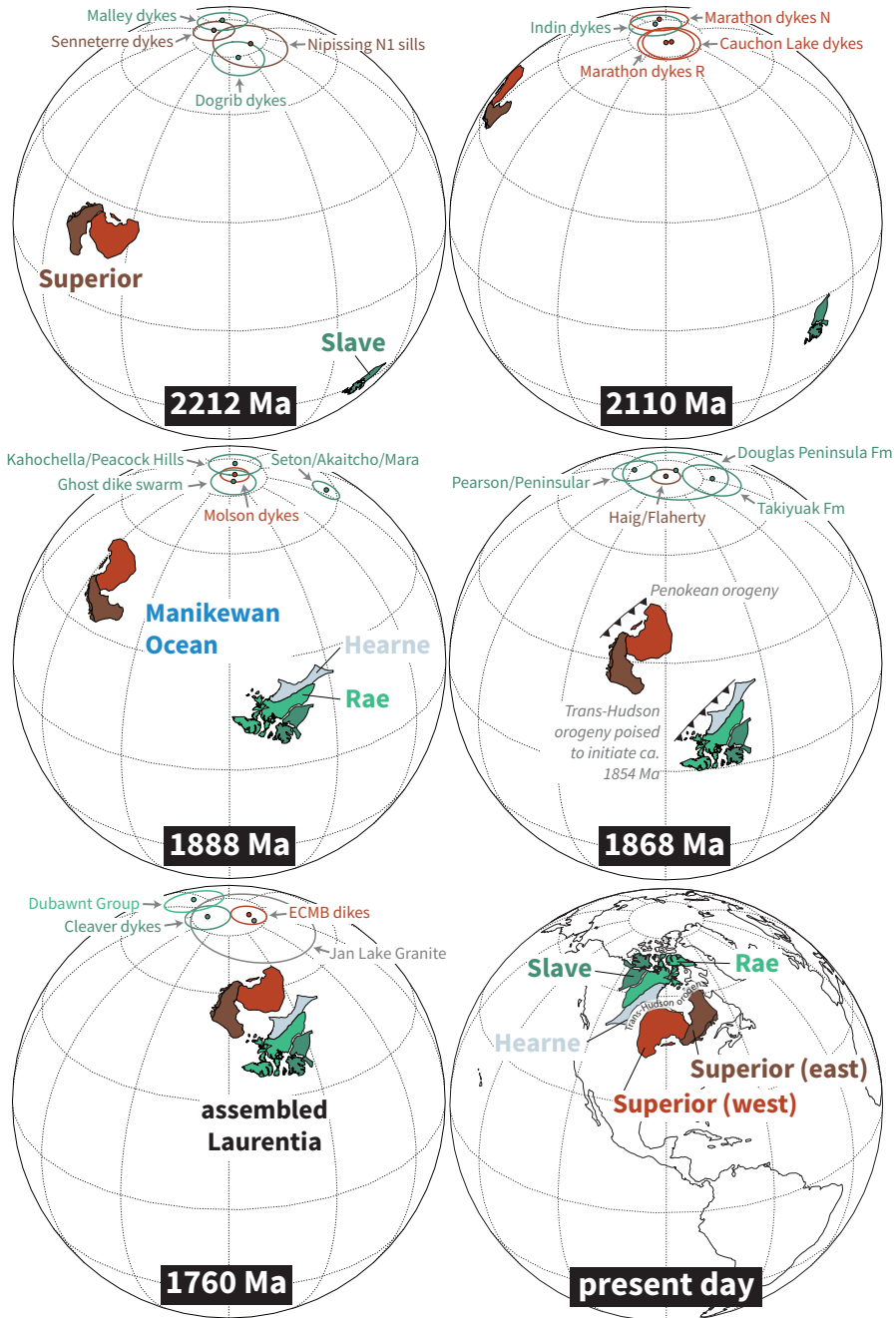


Figure 9. Paleogeographic reconstructions at five different times in the Paleoproterozoic and the position of the provinces at present. Paleomagnetic poles within 20 Myr of the given time (10 Myr for 1888 and 1868 Ma) are shown from the compilation of Evans et al. (2021) as well as the new ECMB pole. These data illustrate differential plate motion between the Superior and Slave Provinces that is required by the data leading up to the closure of the Manikewan Ocean and the assembly of Laurentia during the Trans-Hudson orogeny. The ECMB pole is consistent with an assembled Laurentia following the Trans-Hudson orogeny which contrasts with the disparate orientations and paleolatitudes between Laurentia's constituent provinces prior to the orogeny.

506 Weller & St-Onge, 2017). Geologic data on the timing of Trans-Hudson orogenesis in-
 507 clude a $^{206}\text{Pb}/^{238}\text{U}$ date of 1854.2 ± 1.6 Ma from the base of a foredeep sedimentary suc-
 508 cession on the northern margin of the East Superior province that constrains flexural sub-
 509 sidence associated with Trans-Hudson orogenesis to have initiated at that time (Hodgskiss
 510 et al., 2019). This timing of orogenesis is consistent with $^{207}\text{Pb}/^{206}\text{Pb}$ dates of monazite
 511 within garnet of Trans-Hudson orogen eclogites for which a mean date of 1831 ± 5 Ma
 512 has been interpreted to record peak metamorphism (Weller & St-Onge, 2017). A sim-
 513 ilar timing of *ca.* 1860 to 1820 Ma peak Trans-Hudson metamorphism resulting from col-
 514 lisional orogenesis has been interpreted from U-Pb zircon rim and monazite dates from
 515 the orogen in Baffin Island, Nunavut, Canada (Skipton et al., 2016). These geologic data
 516 strongly support that the Superior Province was conjoined with the Slave + Rae + Hearne
 517 provinces prior to 1800 Ma in their present-day relative positions (Fig. 1). There are high-
 518 quality paleomagnetic poles for the Superior province during the time interval when the
 519 Manikewan Ocean was closing leading up to the Trans-Hudson orogeny (the *ca.* 1880 Mol-
 520 son dykes pole and the *ca.* 1870 Ma Haig/Flaherty pole; Fig. 9). There are no Paleo-
 521 proterozoic paleomagnetic poles for the Superior Province during or after the Trans-Hudson
 522 orogeny that can test Laurentia's coherency with paleomagnetic data. The new 1779.1
 523 ± 2.3 Ma ECMB paleomagnetic pole fills this gap.

524 While abundant paleomagnetic data have been developed from rocks within the
 525 Trans-Hudson orogen (Symons & Harris, 2005), both the primary nature of the rema-
 526 nance directions as well as the age of remanence acquisition has been challenging to es-
 527 tablish. As a result, relatively few poles from this interval during and following Lauren-
 528 tia's amalgamation have been included in curated pole compilations such as that com-
 529 piled by the Nordic paleogeography workshops (Evans et al., 2021). The best constrained
 530 of these poles comes from the post-orogenic 1740 ± 5 Ma Cleaver Dykes of the Great
 531 Bear Magmatic Arc on the western margin of the Slave Province (Fig. 1; Irving (2004)).
 532 The age of these dikes is constrained by a U-Pb baddeleyite date and there is a positive
 533 baked contact test supporting the interpretation that the pole is primary. As can be seen
 534 in Figure 6, the position of this *ca.* 1740 Ma Cleaver Dykes pole for Laurentia (Irving,
 535 2004) is similar to the new pole for the *ca.* 1780 Ma ECMB diabase dikes (Fig. 6). They
 536 do not share a common mean (as determined through Watson and bootstrap common
 537 mean tests; Tauxe et al. (2016)), but are within 11° of one another (less when consid-

538 ering uncertainty). The similarity in these pole positions provides an independent test
 539 of the coherency of the Laurentia craton at that time.

540 An additional pole for comparison comes from hematite remanence of volcanics and
 541 sediments of the Baker Lake Group of the Dubawnt Supergroup which were deposited
 542 in a basin atop the suture between the Rae and Hearne provinces (Figs. 1 and 6; Park
 543 et al. (1973)). Both the depositional age of the succession and the age of hematite re-
 544 manence are roughly constrained leading to a wide assigned age range of 1820 to 1750
 545 Ma in Evans et al. (2021) for the pole. While the loose age constraints hinder firm com-
 546 parisons, the broad similarity of this pole with the Cleaver Dykes pole of the Slave Province
 547 as well as that for Martin Formation (1818 ± 4 Ma) and the Sparrow dikes (1827 ± 4
 548 Ma) of the Rae Province establishes a largely consistent position of the Churchill plate
 549 from *ca.* 1820 to 1740 Ma.

550 A less robust pole for comparison with the new ECMB pole comes from the post-
 551 orogenic Jan Lake Granite within the Trans-Hudson orogen in southeast Saskatchewan
 552 developed in Gala et al. (1995). A U-Pb zircon date of 1758 ± 1 Ma for this granite was
 553 reported in Bickford et al. (2005). Directional data from the Jan Lake Granite falls into
 554 two groups. Based on thermal demagnetization behavior, Irving (2004) interpreted the
 555 ‘A’ grouping to be a TRM held by magnetite that was acquired at the time of the em-
 556 placement of the intrusion *ca.* 1758 Ma. The ECMB dikes pole shares a common mean
 557 with this Jan Lake Granite pole with overlapping A_{95} confidence circles (Fig. 6). This
 558 result is consistent with both the Jan Lake Granite and ECMB being post-orogenic mag-
 559 matic events that occurred following the amalgamation of Laurentia. This similarity sug-
 560 gests that despite the large uncertainty on the Jan Lake Granite pole and the ambigu-
 561 ity resulting from multiple directional groups that the pole does constrain the position
 562 of Laurentia *ca.* 1758 Ma.

563 A pole that does not hold up to such comparative scrutiny is that developed for
 564 the Deschambault Pegmatites from within the Trans-Hudson orogen (Fig. 6C; Symons
 565 et al. (2000)). This pole has been interpreted to constrain the position of Laurentia *ca.*
 566 1766 Ma — an age based on U-Pb monazite and allanite dates of other pegmatites in
 567 the region. As noted in D’Agrella-Filho et al. (2020), there are no field tests for this pole
 568 and the remanence directions from which it is calculated are quite close to the modern
 569 geomagnetic field. This pole was included in the curated Nordic paleogeography work-

shop compilation of Evans et al. (2021) less because of the quality of the individual pole, but rather because there are a number poles of similar position to this one from the Trans-Hudson orogen (Fig. 6). Many of these poles have individual VGPs that are streaked between directions similar to the Jan Lake Granite and that of the present-local field. The direction of the Deschambault pole is far from the new *ca.* 1780 Ma ECMB dikes pole. In contrast, the similarity of pole position between the new ECMB dikes pole and the *ca.* 1758 Ma Jan Lake Granite pole as well as the *ca.* 1740 Ma Cleaver Dykes pole supports that these poles, rather than the Deschambault Pegmatites pole, constrain Laurentia's position during this interval. This Deschambault Pegmatites pole played a role, in conjunction with other poles from the Trans-Hudson orogen, such as that from the Wapisu gneiss and the Deschambault Post pluton, in an interpretation that Laurentia's pole path was at a standstill in the vicinity of the Deschambault Pegmatites pole from *ca.* 1800 Ma through to *ca.* 1766 Ma (Symons et al., 2000; Symons & Harris, 2005). As reviewed in Raub (2008), there are numerous difficulties in interpreting these data from the Trans-Hudson orogen as useful constraints including: 1) a lack of field tests; 2) uncertainty in the timescale of cooling and the timing of the acquisition of magnetization in these slowly cooled units; 3) poorly constrained tilt corrections and 4) large secondary viscous remanent magnetizations that are prevalent due to the coarse grain-size of the igneous lithologies. The preferred interpretation of Raub (2008), which is echoed in D'Agrella-Filho et al. (2020), is that there is unresolved component mixing between primary directions (which would be in the vicinity of the Jan Lake Granite A Group pole and our new ECMB pole) and the present-day north pole as the result of unresolved viscous overprints (Fig. 6). This component mixing leads to streaked site mean directions in individual studies as well as the database of Trans-Hudson orogen poles including the Deschambault Pegmatites pole (Fig. 6; Raub (2008)). The new ECMB pole significantly strengthens this interpretation by demonstrating that a proposed northerly apparent polar wander path to satisfy the Deschambault Pegmatites pole and other Trans-Hudson orogen poles streaked between the Jan Lake Granite and the modern-day pole is indeed fictitious (Fig. 6). Instead, the ECMB pole and the Cleaver Dykes pole establish the paleogeographic position of Laurentia to have been consistent *ca.* 1780 to 1740 Ma (Fig. 9).

601 **6.3 The paleogeography of Laurentia**

602 As is expected by the geologic record of Trans-Hudson orogenesis, the similarity
 603 in pole positions from the southeastern margin of the Superior Provinces (the new ECMB
 604 pole) and the northwestern margin of the Slave Province (the Cleaver Dykes pole; Fig.
 605 6) indicate a coherent assembled Laurentia following 1.8 Ga (Fig. 9). The coherency of
 606 the record of high-quality paleomagnetic poles at this time when the geologic record in-
 607 dicates a recently assembled Laurentia increases confidence that differing pole positions
 608 between Laurentia's Archean provinces earlier in the Paleoproterozoic are indeed a record
 609 of differential plate tectonic motion (Fig. 9). There is a particularly rich record of pa-
 610 leomagnetic poles from the Archean Superior and Slave provinces that can be paired be-
 611 tween 2.23 and 1.89 Ga that constrain the provinces to not be in their modern relative
 612 orientation and to be undergoing differential motion (Mitchell et al., 2014; Buchan et
 613 al., 2016; Swanson-Hysell, 2021). These poles result in reconstructions where prior to the
 614 Trans-Hudson orogeny there was an ocean basin between the Superior province and the
 615 Hearne + Rae + Slave provinces known as the Manikewan Ocean (Fig. 9; Stauffer (1984)).
 616 The poles are consistent with the Superior Province approaching the joint Slave + Hearne
 617 + Rae provinces prior to the onset of the Trans-Hudson orogeny (Fig. 9). These data
 618 provide strong evidence for mobile lid plate tectonics from 2.23 Ga onward (Mitchell et
 619 al., 2014; Buchan et al., 2016; Swanson-Hysell, 2021).

620 The orogenesis associated with Laurentia's assembly is hypothesized to have re-
 621 sulted in the formation of the supercontinent, or semi-supercontinent, Nuna (Hoffman,
 622 1997; Evans & Mitchell, 2011; Evans et al., 2016). Given that Laurentia is the largest
 623 craton hypothesized to have been part of this supercontinent, its paleogeographic po-
 624 sition is key to reconstructions of Nuna. The new ECMB pole provides higher confidence
 625 in the paleogeographic position of Laurentia in the time just following its formation from
 626 the collision of constituent Archean provinces (Fig. 9). This new pole can be used to eval-
 627 uate hypothesized connections between Laurentia and other cratons. There is an increas-
 628 ingly rich global database of paleomagnetic poles *ca.* 1780 Ma including poles from the
 629 Amazonia, Baltica, India, Rio de la Plata, São Francisco and North China cratons (Zhang
 630 et al., 2012; Xu et al., 2014; Bispo-Santos et al., 2014; Shankar et al., 2018; D'Agrella-
 631 Filho et al., 2020).

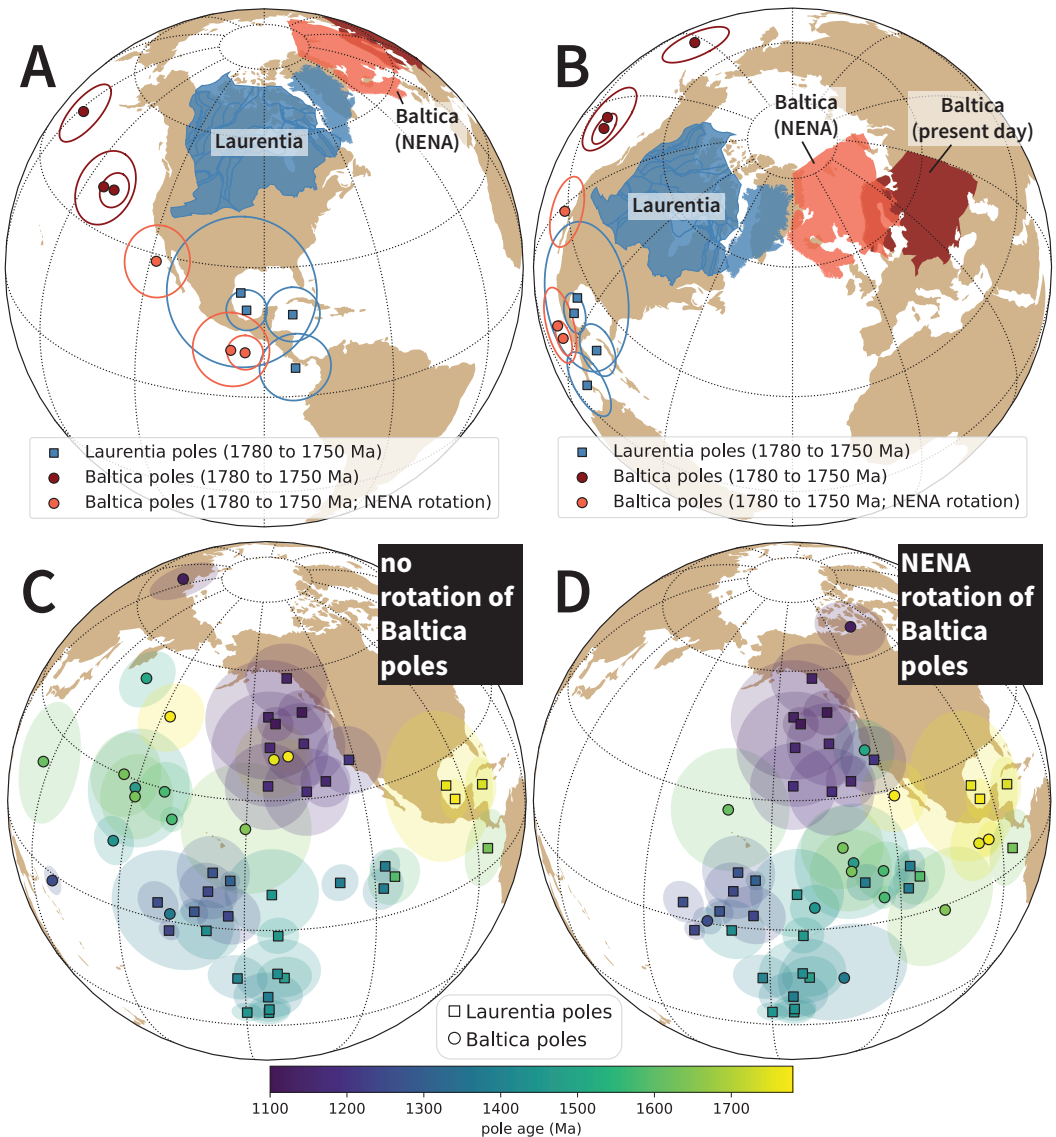


Figure 10. A) Paleomagnetic poles for Laurentia and Baltica between 1780 and 1750 Ma with the Baltica poles shown with and without the NENA rotation (Euler pole for Baltica of $[47.5^\circ, 001.5^\circ, +49.0^\circ]$ as in Evans and Pisarevsky (2008)). Baltica is shown in its present day location in dark red and shown in the NENA position in light red. B) Same data as in panel A shown with a different center of projection which allows for easier visualization of the reconstructed position. C,D) Comparison between poles between 1780 and 1110 Ma between Baltica and Laurentia without (C) and with (D) the NENA rotation. The poles that are shown are those from the Nordic compilation with 'A' and 'B' grades as well as the new ECMB pole from this study.

One hypothesized connection of particular interest is that with Baltica. The two cratons have been hypothesized to have been conjoined such that they shared a margin with a long-lived history of accretionary orogenesis (Hoffman, 1997; Karlstrom et al., 2001). The proposed NENA (northern Europe and North America) configuration between Lau-

636 rentia and Baltica allows for such a shared margin (Gower et al., 1990; Buchan et al.,
 637 2000; Evans & Pisarevsky, 2008). The increased concordance between *ca.* 1780 to 1750
 638 paleomagnetic poles from Laurentia and Baltica upon the NENA rotation of Baltica can
 639 be seen in Figure 10. Paleomagnetic poles support a continued NENA connection un-
 640 til at least 1260 Ma (supported by poles from Baltica's *ca.* 1258 Ma post-Jotnian intru-
 641 sions and Laurentia's *ca.* 1267 Ma Mackenzie dikes) and perhaps to 1120 Ma (where the
 642 paleomagnetic comparison is reliant on the *ca.* 1122 Ma Salla dike of Baltica developed
 643 from a single cooling unit; Salminen et al. (2009)). This connection supports the long-
 644 lived active margin where Laurentia grew through the rest of the Paleoproterozoic and
 645 through the Mesoproterozoic until the *ca.* 1.08 Ga continent-continent collision of the
 646 Grenvillian orogeny (Whitmeyer & Karlstrom, 2007).

647 7 Conclusions

648 The East-Central Minnesota Batholith was emplaced following Penokean oroge-
 649 nesis on the southeast margin of the Superior Province. While the southeast margin of
 650 Laurentia experienced subsequent intervals of accretionary orogenesis, thermochronol-
 651 ogy data constrain the batholith to have a straight-forward history of post-emplacement
 652 rapid exhumation without substantial reheating. Subsequent orogenesis occurred well
 653 southeast of the batholith — consistent with the batholith having played a role in sta-
 654 bilizing Laurentian lithosphere. Comagmatic diabase dikes of the East-Central Minnesota
 655 Batholith can be constrained through U-Pb geochronology on the felsic units to have been
 656 emplaced at 1779.1 ± 2.3 Ma. A new paleomagnetic pole developed from the magnetite
 657 remanence of these dikes provides a high-quality constraint on the position of Lauren-
 658 tia following Trans-Hudson orogenesis. This pole confirms the coherency of an amalgा-
 659 mated Laurentia at the time and supports the NENA connection with Baltica. This pa-
 660 leomagnetic coherency further strengthens the case that previously disparate pole po-
 661 sitions between the Superior and Slave provinces are the result of *ca.* 2.2 to 1.8 Ga mobile-
 662 lid plate tectonics. The geologic and paleomagnetic record of Laurentia is inconsistent
 663 with a stagnant-lid regime anytime over the past 2.2 billion years.

664 Acknowledgments

665 This research was supported by the National Science Foundation through CAREER grant
 666 EAR-1847277 awarded to N.L.S.-H.. Rock magnetic experiments using the MPMS were

conducted at the Institute for Rock Magnetism which is supported by the Instrumentation and Facilities program of the National Science Foundation, Earth Science Division. We gratefully acknowledge Mark Schmitz and Jim Crowley for analytical support at the Boise State Isotope Geology Laboratory. Noah McLean provided insight for the methodology applied to interpret the uncertainty associated with the age of a unit bracketed by U-Pb dates. We thank Stearns County Parks for research permits that enabled sample collection in Quarry Park and Nature Preserve. The manuscript was improved through thoughtful reviews from Daniel Holm, Anthony Pivarunas, and an anonymous reviewer. Paleomagnetic data associated with this study are available within the MagIC database (<https://earthref.org/MagIC/17072/162b766f-435a-4053-bf63-0a5246c24339>; UPDATE TO DOI WHEN ASSIGNED) and all data are within a Github repository associated with this work (https://github.com/Swanson-Hysell-Group/2021_ECMB) that is also archived on Zenodo (<https://doi.org/10.5281/zenodo.4625041>). This repository also contains Python code related to calculations, visualizations and statistical tests discussed herein.

References

- Ague, J. J. (1997). Thermodynamic calculation of emplacement pressures for batholithic rocks, California: Implications for the aluminum-in-hornblende barometer. *Geology*, 25(6), 563. doi: 10.1130/0091-7613(1997)025<0563:tcoepf>2.3.co;2
- Besnus, M. J., & Meyer, A. J. (1964). Nouvelles données expérimentales sur le magnétisme de la pyrrhotine naturelle. In *Proc. int. conf. mag.* (Vol. 20, p. 507-511).
- Bickford, M. E., Mock, T. D., Steinhart III, W. E., Collerson, K. D., & Lewry, J. F. (2005). Origin of the Archean Sask craton and its extent within the Trans-Hudson orogen: evidence from Pb and Nd isotopic compositions of basement rocks and post-orogenic intrusions. *Canadian Journal of Earth Sciences*, 42, 659–684. doi: 10.1139/e04-064
- Bispo-Santos, F., D’Agrella-Filho, M. S., Trindade, R. I., Janikian, L., & Reis, N. J. (2014). Was there SAMBA in Columbia? Paleomagnetic evidence from 1790 Ma Avanavero mafic sills (northern Amazonian Craton). *Precambrian Research*, 244, 139–155. doi: 10.1016/j.precamres.2013.11.002

- 699 Boerboom, T. J., & Holm, D. K. (2000). Paleoproterozoic Intrusive Igneous Rocks of
700 Southeastern Stearns County, Central Minnesota. *Minnesota Geological Survey*
701 *Report of Investigations 56.*
- 702 Boerboom, T. J., Holm, D. K., & Van Schmus, R. (2011). Late Paleoproterozoic
703 deformational, metamorphic, and magmatic history of east-central Minnesota.
704 *Archean to Anthropocene: Field Guides to the Geology of the Mid-Continent of*
705 *North America*, 1–23. doi: 10.1130/2011.0024(01)
- 706 Boerboom, T. J., Holm, D. K., & Van Schmus, W. R. (2005). Granites of the East-
707 Central Minnesota Batholith. *Minnesota Geological Survey Guidebook*.
- 708 Boerboom, T. J., Setterholm, D. R., & Chandler, V. W. (1995). Bedrock geology pl.
709 2. In G. N. Meyer (Ed.), *Geologic atlas of Stearns County, Minnesota: Min-*
710 *nnesota Geological Survey County Atlas C-10, pt. A., 7 pls., scales 1:100,000*
711 *and 1:200,000*. Minnesota Geological Survey.
- 712 Buchan, K. L., Mertanen, S., Park, R., Pesonen, L., Elming, S. A., Abrahamsen, N.,
713 & Bylund, G. (2000). Comparing the drift of Laurentia and Baltica in the
714 Proterozoic: the importance of key paleomagnetic poles. *Tectonophysics*, 319,
715 167–198. doi: 10.1016/S0040-1951(00)00032-9
- 716 Buchan, K. L., Mitchell, R. N., Bleeker, W., Hamilton, M. A., & LeCheminant,
717 A. N. (2016). Paleomagnetism of ca. 2.13–2.11 Ga Indin and ca. 1.885
718 Ga Ghost dyke swarms of the Slave craton: Implications for the Slave
719 craton APW path and relative drift of Slave, Superior and Siberian cra-
720 tons in the Paleoproterozoic. *Precambrian Research*, 275, 151–175. doi:
721 10.1016/j.precamres.2016.01.012
- 722 Chamberlain, K. R., & Bowring, S. A. (2001). Apatite–feldspar U–Pb ther-
723 mochonometer: a reliable, mid-range ($\sim 450^{\circ}\text{C}$), diffusion-controlled system.
724 *Chemical Geology*, 172(1-2), 173–200. doi: 10.1016/s0009-2541(00)00242-4
- 725 Cherniak, D., Lanford, W., & Ryerson, F. (1991). Lead diffusion in apatite
726 and zircon using ion implantation and Rutherford backscattering tech-
727 niques. *Geochimica et Cosmochimica Acta*, 55(6), 1663–1673. doi:
728 10.1016/0016-7037(91)90137-t
- 729 Cherniak, D., & Watson, E. (2001). Pb diffusion in zircon. *Chemical Geology*, 172(1-
730 2), 5–24. doi: 10.1016/s0009-2541(00)00233-3
- 731 Cochrane, R., Spikings, R. A., Chew, D., Wotzlaw, J.-F., Chiaradia, M., Tyrrell, S.,

- 732 ... der Lelij, R. V. (2014). High temperature ($>350^{\circ}\text{C}$) thermochronology and
733 mechanisms of Pb loss in apatite. *Geochimica et Cosmochimica Acta*, 127,
734 39–56. doi: 10.1016/j.gca.2013.11.028
- 735 Corrigan, D., Pehrsson, S., Wodicka, N., & de Kemp, E. (2009). The Palaeoproterozoic
736 Trans-Hudson Orogen: a prototype of modern accretionary processes. *Geological Society,
737 London, Special Publications*, 327(1), 457–479. doi: 10.1144/
738 sp327.19
- 739 D'Agrella-Filho, M. S., Teixeira, W., da Trindade, R. I., Patroni, O. A., & Prieto,
740 R. F. (2020). Paleomagnetism of 1.79 Ga Pará de Minas mafic dykes: Testing
741 a São Francisco/Congo-North China-Rio de la Plata connection in Columbia.
742 *Precambrian Research*, 338, 105584. doi: 10.1016/j.precamres.2019.105584
- 743 Deenen, M. H. L., Langereis, C. G., van Hinsbergen, D. J. J., & Biggin, A. J.
744 (2011). Geomagnetic secular variation and the statistics of palaeomag-
745 netic directions. *Geophysical Journal International*. doi: 10.1111/
746 j.1365-246X.2011.05050.x
- 747 Dewane, T., & Van Schmus, W. (2007). U-Pb geochronology of the Wolf River
748 batholith, north-central Wisconsin: Evidence for successive magmatism be-
749 tween 1484 Ma and 1468 Ma. *Precambrian Research*, 157(1-4), 215–234. doi:
750 10.1016/j.precamres.2007.02.018
- 751 Dodson, M. H. (1973). Closure temperature in cooling geochronological and petro-
752 logical systems. *Contributions to Mineralogy and Petrology*, 40(3), 259–274.
753 doi: 10.1007/bf00373790
- 754 Evans, D. A. D., Li, Z. X., & Murphy, J. B. (2016). Four-dimensional context of
755 Earth's supercontinents. In D. A. D. Evans, Z. X. Li, & J. B. Murphy (Eds.),
756 *Supercontinent cycles through earth history* (Vol. 424). Geological Society, Lon-
757 don, Special Publications. doi: 10.1144/SP424.12
- 758 Evans, D. A. D., & Mitchell, R. N. (2011). Assembly and breakup of the core of
759 Paleoproterozoic–Mesoproterozoic supercontinent Nuna. *Geology*, 39, 443–446.
760 doi: 10.1130/G31654.1
- 761 Evans, D. A. D., Pesonen, L. J., Eglington, B. M., Elming, S.-Å., Gong, Z., Li, Z.-
762 X., ... Zhang, S. (2021). An expanding list of reliable paleomagnetic poles
763 for Precambrian tectonic reconstructions. In L. J. Pesonen, D. A. D. Evans,
764 S. Å. Elming, J. M. Salminen, & T. Veikkolainen (Eds.), *Ancient superconti-*

- 765 nents and the paleogeography of the earth. Elsevier.
- 766 Evans, D. A. D., & Pisarevsky, S. A. (2008). Plate tectonics on early Earth? weighing
767 the paleomagnetic evidence. *Geological Society of America Special Papers*,
768 440, 249–263. doi: 10.1130/2008.2440(12)
- 769 Fairchild, L. M., Swanson-Hysell, N. L., Ramezani, J., Sprain, C. J., & Bowring,
770 S. A. (2017). The end of Midcontinent Rift magmatism and the paleogeogra-
771 phy of Laurentia. *Lithosphere*, 9(1), 117-133. doi: 10.1130/L580.1
- 772 Feinberg, J., Solheid, P., Swanson-Hysell, N., Jackson, M., & Bowles, J. (2015).
773 Full vector low-temperature magnetic measurements of geologic materials.
- 774 *Geochemistry, Geophysics, Geosystems*, 16, 301–314. doi: 2014GC005591
- 775 Fisher, N. I., Lewis, T., & Embleton, B. J. J. (1987). *Statistical analysis of spherical*
776 *data*. Cambridge University Press. doi: 10.1017/CBO9780511623059
- 777 Gala, M. G., Symons, D. T. A., & Palmer, H. C. (1995). Paleomagnetism of the
778 Jan Lake Granite, Trans-Hudson Orogen. *Saskatchewan Geological Survey*
779 *Summary of Investigations*, 95-4.
- 780 Gower, C. F., Ryan, A. B., & Rivers, T. (1990). Mid-Proterozoic Laurentia-Baltica:
781 An overview of its geological evolution and a summary of the contributions
782 made by this volume. In C. F. Gower, T. Rivers, & A. B. Ryan (Eds.), *Mid-*
783 *Proterozoic Laurentia-Baltica*. Geological Association of Canada, Special
784 Paper.
- 785 Grove, M., & Harrison, T. M. (1996). $^{40}\text{Ar}^*$ diffusion in Fe-rich biotite. *American*
786 *Mineralogist*, 81, 940–951. doi: 10.2138/am-1996-7-816
- 787 Hanson, G. (1968). K-Ar ages for hornblende from granites and gneisses and for
788 basaltic intrusives in Minnesota. *Minnesota Geological Survey Report of Inves-*
789 *tigations*, 8.
- 790 Harrison, T. M. (1982). Diffusion of ^{40}Ar in hornblende. *Contributions to Mineralogy*
791 *and Petrology*, 78(3), 324–331. doi: 10.1007/BF00398927
- 792 Hodgskiss, M. S., Dagnaud, O. M., Frost, J. L., Halverson, G. P., Schmitz, M. D.,
793 Swanson-Hysell, N. L., & Sperling, E. A. (2019). New insights on the Orosirian
794 carbon cycle, early cyanobacteria, and the assembly of Laurentia from the
795 Paleoproterozoic Belcher Group. *Earth and Planetary Science Letters*, 520,
796 141–152. doi: 10.1016/j.epsl.2019.05.023
- 797 Hoffman, P. F. (1988). United plates of America, the birth of a craton: Early Pro-

- terozoic assembly and growth of Laurentia. *Annual Review of Earth and Planetary Sciences*, 16(1), 543-603. doi: 10.1146/annurev.ea.16.050188.002551

Hoffman, P. F. (1997). Tectonic genealogy of North America. In B. van der Pluijm & S. Marshak (Eds.), *Earth structure: An introduction to structural geology and tectonics* (p. 459-464). McGraw-Hill.

Holm, D. K., Anderson, R., Boerboom, T., Cannon, W., Chandler, V., Jirsa, M., ... Van Schmus, W. (2007). Reinterpretation of Paleoproterozoic accretionary boundaries of the north-central United States based on a new aeromagnetic-geologic compilation. *Precambrian Research*, 157(1-4), 71-79. doi: 10.1016/j.precamres.2007.02.023

Holm, D. K., Darrah, K. S., & Lux, D. R. (1998). Evidence for widespread approximately 1760 Ma metamorphism and rapid crustal stabilization of the early Proterozoic (1870-1820 Ma) Penokean Orogen, Minnesota. *American Journal of Science*, 298(1), 60-81. doi: 10.2475/ajs.298.1.60

Holm, D. K., Gordon Medaris, L., McDannell, K. T., Schneider, D. A., Schulz, K., Singer, B. S., & Jicha, B. R. (2019). Growth, overprinting, and stabilization of Proterozoic Provinces in the southern Lake Superior region. *Precambrian Research*. doi: 10.1016/j.precamres.2019.105587

Holm, D. K., & Lux, D. R. (1996). Core complex model proposed for gneiss dome development during collapse of the Paleoproterozoic Penokean orogen, Minnesota. *Geology*, 24(4), 343. doi: 10.1130/0091-7613(1996)024<0343:ccmpfg>2.3.co;2

Holm, D. K., Schneider, D., & Coath, C. D. (1998). Age and deformation of Early Proterozoic quartzites in the southern Lake Superior region: Implications for extent of foreland deformation during final assembly of Laurentia. *Geology*, 26(10), 907. doi: 10.1130/0091-7613(1998)026<0907:aadoep>2.3.co;2

Holm, D. K., & Selverstone, J. (1990). Rapid growth and strain rates inferred from synkinematic garnets, Penokean orogeny, Minnesota. *Geology*, 18(2), 166. doi: 10.1130/0091-7613(1990)018<0166:rgasri>2.3.co;2

Holm, D. K., Van Schmus, W. R., MacNeill, L. C., Boerboom, T. J., Schweitzer, D., & Schneider, D. (2005). U-Pb zircon geochronology of Paleoproterozoic plutons from the northern midcontinent, USA: Evidence for subduction flip and continued convergence after geon 18 Penokean orogenesis. *Geological Society of America Special Paper*, 437, 1-32. doi: 10.1130/2005.2437

- America Bulletin, 117(3), 259–275. doi: 10.1130/b25395.1

Horan, M. F., Hanson, G. N., & Spencer, K. J. (1987). Pb and Nd isotope and trace element constraints on the origin of basic rocks in an early Proterozoic igneous complex, Minnesota. *Precambrian Research*, 37(4), 323–342. doi: 10.1016/0301-9268(87)90081-7

Irving, E. (2004). Early Proterozoic geomagnetic field in western Laurentia: implications for paleolatitudes, local rotations and stratigraphy. *Precambrian Research*, 129(3-4), 251–270. doi: 10.1016/j.precamres.2003.10.002

Jirsa, M., Boerboom, T., & Chandler, V. (2012). S-22, *Geologic Map of Minnesota, Precambrian Bedrock Geology* (Tech. Rep.). Minnesota Geological Survey.

Karlstrom, K. E., Ahall, K.-I., Harlan, S. S., Williams, M. L., McLelland, J., & Geissman, J. W. (2001). Long-lived (1.8-1.0 Ga) convergent orogen in southern Laurentia, its extensions to Australia and Baltica, and implications for refining Rodinia. *Precambrian Research*, 111(1-4), 5–30. doi: 10.1016/S0301-9268(01)00154-1

Kissin, S. A., & Scott, S. D. (1982). Phase relations involving pyrrhotite below 350°C. *Economic Geology*, 77(7), 1739–1754. doi: 10.2113/gsecongeo.77.7.1739

Ludwig, K. (1998). On the treatment of concordant uranium-lead ages. *Geochimica Cosmochimica Acta*, 62, 665–676.

Medaris, L. G., Singer, B. S., Jicha, B. R., Malone, D. H., Schwartz, J. J., Stewart, E. K., ... Reiners, P. W. (2021). Early Mesoproterozoic evolution of midcontinental Laurentia: Defining the geon 14 Baraboo orogeny. *Geoscience Frontiers*, 12(5), 101174. doi: 10.1016/j.gsf.2021.101174

Meert, J. G., Pivarunas, A. F., Evans, D. A., Pisarevsky, S. A., Pesonen, L. J., Li, Z.-X., ... Salminen, J. M. (2020). The magnificent seven: A proposal for modest revision of the quality index. *Tectonophysics*, 790, 228549. doi: 10.1016/j.tecto.2020.228549

Mitchell, R. N., Bleeker, W., van Breemen, O., Lecheminant, T. N., Peng, P., Nilsson, M. K. M., & Evans, D. A. D. (2014). Plate tectonics before 2.0 Ga: Evidence from paleomagnetism of cratons within supercontinent Nuna. *American Journal of Science*, 314(4), 878–894. doi: 10.2475/04.2014.03

Mutch, E. J. F., Blundy, J. D., Tatttitch, B. C., Cooper, F. J., & Brooker, R. A.

- 864 (2016). An experimental study of amphibole stability in low-pressure granitic
865 magmas and a revised Al-in-hornblende geobarometer. *Contributions to Mineralogy and Petrology*, 171(10). doi: 10.1007/s00410-016-1298-9
- 866
- 867 Park, J. K., Irving, E., & Donaldson, J. A. (1973). Paleomagnetism of the Precambrian Dubawnt Group. *Geological Society of America Bulletin*, 84(3), 859-870.
868 doi: 10.1130/0016-7606(1973)84<859:potpdg>2.0.co;2
- 869
- 870 Pehrsson, S. J., Eglington, B. M., Evans, D. A. D., Huston, D., & Reddy, S. M.
871 (2015). Metallogeny and its link to orogenic style during the Nuna supercontinent cycle. *Geological Society, London, Special Publications*, 424, 83-94. doi:
872 10.1144/SP424.5
- 873
- 874 Raub, T. M. (2008). *Paleomagnetism of Dubawnt Supergroup, Baker Lake Basin, Nunavut, Canada: Refining Laurentia's Paleoproterozoic apparent polar wander path* (Unpublished doctoral dissertation). Yale University.
- 875
- 876
- 877 Rothstein, D. A., & Manning, C. E. (2003). Geothermal gradients in continental
878 magmatic arcs; constraints from the eastern Peninsular Ranges Batholith,
879 Baja California, Mexico. *Tectonic evolution of northwestern Mexico and the Southwestern USA, Geological Society of America Special Paper*, 374. doi:
880 10.1130/0-8137-2374-4.337
- 881
- 882 Salminen, J., Pesonen, L. J., Mertanen, S., Vuollo, J., & Airo, M.-L. (2009). Palaeomagnetism of the Salla Diabase Dyke, northeastern Finland, and its implication for the Baltica-Laurentia entity during the Mesoproterozoic. *Geological Society, London, Special Publications*, 323(1), 199-217. doi: 10.1144/SP323.9
- 883
- 884
- 885
- 886 Schmitz, M., Southwick, D., Bickford, M., Mueller, P., & Samson, S. (2018).
887 Neoarchean and Paleoproterozoic events in the Minnesota River Valley
888 subprovince, with implications for southern Superior craton evolution
889 and correlation. *Precambrian Research*, 316, 206–226. doi: 10.1016/j.precamres.2018.08.010
- 890
- 891 Schoene, B., & Bowring, S. A. (2007). Determining accurate temperature-time
892 paths from U-Pb thermochronology: An example from the Kaapvaal craton,
893 southern Africa. *Geochimica et Cosmochimica Acta*, 71(1), 165–185. doi:
894 10.1016/j.gca.2006.08.029
- 895
- 896 Schulz, K. J., & Cannon, W. F. (2007). The Penokean orogeny in the Lake Superior region. *Precambrian Research*, 157(1-4), 4–25. doi: 10.1016/j.precamres.2007

- 897 .02.022
- 898 Shankar, R., Sarma, D. S., Babu, N. R., & Parashuramulu, V. (2018). Paleomag-
899 netic study of 1765 Ma dyke swarm from the Singhbum Craton: Implications
900 to the paleogeography of India. *Journal of Asian Earth Sciences*, 157, 235–244.
901 doi: 10.1016/j.jseaes.2017.08.026
- 902 Skipton, D. R., St-Onge, M. R., Schneider, D. A., & McFarlane, C. R. M. (2016).
903 Tectonothermal evolution of the middle crust in the Trans-Hudson Orogen,
904 Baffin Island, Canada: Evidence from petrology and monazite geochronology
905 of sillimanite-bearing migmatites. *Journal of Petrology*, 57(8), 1437–1462. doi:
906 10.1093/petrology/egw046
- 907 Smye, A., Marsh, J., Vermeesch, P., Garber, J., & Stockli, D. (2018, sep). Ap-
908 plications and limitations of U-Pb thermochronology to middle and lower
909 crustal thermal histories. *Chemical Geology*, 494, 1–18. doi: 10.1016/
910 j.chemgeo.2018.07.003
- 911 Southwick, D. L., Morey, G. B., & Mossler, J. H. (1986). Fluvial origin of the lower
912 proterozoic sioux quartzite, southwestern minnesota. *GSA Bulletin*, 97(12),
913 1432–1441. doi: 10.1130/0016-7606(1986)97<1432:FOOTLP>2.0.CO;2
- 914 Stauffer, M. R. (1984). Manikewan: An early Proterozoic ocean in central Canada,
915 its igneous history and orogenic closure. *Precambrian Research*, 25(1), 257–
916 281. doi: 10.1016/0301-9268(84)90036-6
- 917 Swanson-Hysell, N. L. (2021). The Precambrian Paleogeography of Laurentia. In
918 L. J. Pesonen, D. A. D. Evans, S. Å. Elming, J. M. Salminen, & T. Veikko-
919 lainen (Eds.), *Ancient supercontinents and the paleogeography of the earth*.
920 Elsevier.
- 921 Swanson-Hysell, N. L., Hoaglund, S. A., Crowley, J. L., Schmitz, M. D., Zhang,
922 Y., & Miller, J. D. (2020). Rapid emplacement of massive Duluth Com-
923 plex intrusions within the North American Midcontinent Rift. *Geology*. doi:
924 10.1130/g47873.1
- 925 Swanson-Hysell, N. L., Ramezani, J., Fairchild, L. M., & Rose, I. R. (2019). Failed
926 rifting and fast drifting: Midcontinent Rift development, Laurentia's rapid
927 motion and the driver of Grenvillian orogenesis. *GSA Bulletin*, 131, 913–940.
928 doi: 10.1130/b31944.1
- 929 Symons, D. T. A., & Harris, M. J. (2005). Accretion history of the Trans-Hudson

- Orogen in Manitoba and Saskatchewan from paleomagnetism. *Canadian Journal of Earth Sciences*, 42(4), 723–740. doi: 10.1139/e04-090
- Symons, D. T. A., Symons, T., & Lewchuk, M. (2000). Paleomagnetism of the Deschambault pegmatites: Stillstand and hairpin at the end of the Paleoproterozoic Trans-Hudson Orogeny, Canada. *Physics and Chemistry of the Earth, Part A: Solid Earth and Geodesy*, 25(5), 479–487. doi: 10.1016/s1464-1895(00)00074-0
- Tauxe, L., Shaar, R., Jonestrask, L., Swanson-Hysell, N., Minnett, R., Koppers, A., ... Fairchild, L. (2016). PmagPy: Software package for paleomagnetic data analysis and a bridge to the Magnetics Information Consortium (MagIC) Database. *Geochemistry, Geophysics, Geosystems*, 17, 2450-2463. doi: 10.1002/2016GC006307
- Thébault, E., Finlay, C. C., Beggan, C. D., Alken, P., Aubert, J., Barrois, O., ... Zvereva, T. (2015). International Geomagnetic Reference Field: the 12th generation. *Earth, Planets and Space*, 67(1). doi: 10.1186/s40623-015-0228-9
- Van der Voo, R. (1990, 11 10). The reliability of paleomagnetic data. *Tectonophysics*, 184(1), 1–9. doi: 10.1016/0040-1951(90)90116-P
- Vermesch, P. (2018). IsoplotR: A free and open toolbox for geochronology. *Geoscience Frontiers*, 9(5), 1479–1493. doi: 10.1016/j.gsf.2018.04.001
- Verwey, E. J. W. (1939). Electronic conduction of magnetite (Fe_3O_4) and its transition point at low temperatures. *Nature*, 144, 327-328. doi: 10.1038/144327b0
- Weller, O. M., & St-Onge, M. R. (2017). Record of modern-style plate tectonics in the Palaeoproterozoic Trans-Hudson orogen. *Nature Geoscience*, 10, 305–311. doi: 10.1038/ngeo2904
- Whitmeyer, S., & Karlstrom, K. (2007). Tectonic model for the Proterozoic growth of North America. *Geosphere*, 3(4), 220–259. doi: 10.1130/GES00055.1
- Xu, H., Yang, Z., Peng, P., Meert, J. G., & Zhu, R. (2014). Paleo-position of the North China craton within the supercontinent Columbia: Constraints from new paleomagnetic results. *Precambrian Research*, 255, 276–293. doi: 10.1016/j.precamres.2014.10.004
- Zhang, S., Li, Z.-X., Evans, D. A. D., Wu, H., Li, H., & Dong, J. (2012). Pre-Rodinia supercontinent Nuna shaping up: A global synthesis with new paleomagnetic results from North China. *Earth and Planetary Science Letters*,

963 353–354, 145–155. doi: 10.1016/j.epsl.2012.07.034

Table 1. Summary of site level paleomagnetic data

site	site lat	site lon	n	dec	inc	k	R	α_{95}	VGP lat	VGP lon
<i>northeast-trending dike magnetite-component site means</i>										
NED1	45.53423	265.75804	8	157.6	74.7	380	7.98	2.8	18.4	276.9
NED2	45.53421	265.75816	8	172.3	74.9	420	7.98	2.7	17.4	269.6
NED5	45.53309	265.75803	6	170.3	79.0	213	5.98	4.6	24.5	269.6
NED6	45.53299	265.75773	9	197.8	73.6	183	8.96	3.8	16.1	256.5
NED7	45.53288	265.75767	5	266.3	81.3	204	4.98	5.4	42.0	242.6
NED8	45.53286	265.75782	7	202.6	78.6	423	6.99	2.9	24.8	256.6
NED9	45.53314	265.75855	7	191.1	71.5	90	6.93	6.4	12.2	259.5
NED10	45.53259	265.75742	6	199.7	73.3	324	5.98	3.7	15.8	255.4
NED11	45.53252	265.75768	7	166.1	75.1	391	6.98	3.1	18.1	272.6
NED12	45.53489	265.76076	6	179.5	73.0	374	5.99	3.5	14.1	266.0
NED13	45.53497	265.76113	7	169.1	73.9	199	6.97	4.3	15.9	271.4
NED14	45.53492	265.76119	6	193.0	70.0	217	5.98	4.6	10.1	258.0
NED15	45.53688	265.76758	8	175.8	77.7	604	7.99	2.3	22.0	267.6
NED16	45.53728	265.76822	5	185.1	78.6	449	4.99	3.6	23.6	263.7
NED18	45.53124	265.76945	6	134.7	81.7	159	5.97	5.3	33.2	279.5
NED23	45.53398	265.74200	7	193.0	76.4	411	6.99	3.0	20.2	259.7
NED25	45.53396	265.74119	4	135.4	80.7	334	3.99	5.0	31.5	280.6
NED26	45.53445	265.74129	5	151.1	73.4	572	4.99	3.2	17.4	280.8
NED28	45.53467	265.73817	4	157.8	73.8	145	3.98	7.7	16.9	277.2
NED29	45.53438	265.73690	8	219.0	76.7	119	7.94	5.1	24.4	248.6
NED31	45.53385	265.75785	3	184.7	69.4	1730	3.00	3.0	8.7	262.9
NED34	45.51700	265.78083	8	185.9	77.0	362	7.98	2.9	20.8	263.1
NED35	45.53320	265.75761	8	166.4	74.7	261	7.97	3.4	17.4	272.6
mean pole: pole longitude: 265.8; pole latitude: 20.4; A_{95}: 4.5; K: 45.6 N: 23										
<i>northwest-trending dike magnetite-component site mean</i>										
NWD1	45.53407	265.76852	9	293.4	41.6	66	8.88	6.4	32.9	177.5

Notes: site lat–latitude of site ($^{\circ}$; WGS84); site lon–longitude of site ($^{\circ}$; WGS84) n–number of samples analyzed and included in the site mean; dec–tilt-correction mean declination for the site; inc–tilt-correction mean inclination for the site; k–Fisher precision parameter; R–resultant vector length; α_{95} –95% confidence limit in degrees; VGP lat–latitude of the virtual geomagnetic pole for the site; VGP lon–longitude of the virtual geomagnetic pole for the site.

Table 2. Summary of ID-TIMS $^{207}\text{Pb}/^{206}\text{Pb}$ East-Central Minnesota Batholith zircon dates

Sample	Unit	Latitude	$^{207}\text{Pb}/^{206}\text{Pb}$	Uncertainty (2σ)	MSWD	n/N
		Longitude	date (Ma)	X	Z	
ECMB6	St. Cloud Granite	45.53396° N 94.23187° W	1781.44	0.51	2.4	1.24
QP1	quartz-feldspar porphyry dike	45.53481° N 94.25811° W	1780.78	0.45	2.4	0.53
ECMB4	Richmond Granite	45.44343° N 94.48360° W	1776.76	0.49	2.4	1.15
						7/8

Notes: X is 2σ analytical uncertainty; Z is 2σ uncertainty including decay constant uncertainty. This Z uncertainty needs to be utilized when comparing to dates using other decay systems (e.g., $^{40}\text{Ar}/^{39}\text{Ar}$, $^{187}\text{Re}-^{187}\text{Os}$); MSWD is the mean squared weighted deviation; n is the number of individual zircon dates included in the calculated sample mean date; N is the number of individual zircons analyzed for the sample.